# Shock Waves in Dispersive Eulerian Fluids

**M. A. Hoefer**

**Abstract**  The long-time behavior of an initial step resulting in a dispersive shock wave (DSW) for the one-dimensional isentropic Euler equations regularized by generic, third-order dispersion is considered by use of Whitham averaging. Under modest assumptions, the jump conditions (DSW locus and speeds) for admissible, weak DSWs are characterized and found to depend only upon the sign of dispersion (convexity or concavity) and a general pressure law. Two mechanisms leading to the breakdown of this simple wave DSW theory for sufficiently large jumps are identified: a change in the sign of dispersion, leading to gradient catastrophe in the modulation equations, and the loss of genuine nonlinearity in the modulation equations. Large amplitude DSWs are constructed for several particular dispersive fluids with differing pressure laws modeled by the generalized nonlinear Schrödinger equation. These include superfluids (Bose–Einstein condensates and ultracold fermions) and "optical fluids." Estimates of breaking times for smooth initial data and the long-time behavior of the shock tube problem are presented. Detailed numerical simulations compare favorably with the asymptotic results in the weak to moderate amplitude regimes. Deviations in the large amplitude regime are identified with breakdown of the simple wave DSW theory.

Communicated by M. I. Weinstein.

M. A. Hoefer (✉)
Department of Mathematics, North Carolina State University, Raleigh, NC 27695, USA
e-mail: mahoefer@ncsu.edu

Published online: 27 March 2014

⚡ Springer

## 1 Introduction

Nonlinear wave propagation in dispersive media with negligible dissipation can lead to the formation of dispersive shock waves (DSWs). In contrast to classical, viscous shock waves which are localized, rapid jumps in the fluid's thermodynamic variables, DSWs exhibit an expanding oscillatory region connecting two disparate fluid states. A schematic depicting typical left-going DSWs for positive and negative dispersion fluids is shown in Fig. 1. These structures are of particular, current interest due to their recent observation in superfluidic Bose–Einstein condensates (BECs) of cold atomic gases (Dutton et al. 2001; Simula et al. 2005; Hoefer et al. 2006; Chang et al. 2008; Meppelink et al. 2009) and nonlinear photonics (Wan et al. 2007; Jia et al. 2007; Barsi et al. 2007; Ghofraniha et al. 2007; Conti et al. 2009; Wan et al. 2010; Conforti et al. 2012; Ghofraniha et al. 2012). DSWs also occur in a number of other dispersive hydrodynamic-type systems including water waves (Chanson 2009) (known as undular hydraulic jumps or bores), two-temperature collisionless plasma (Taylor et al. 1970) (called collisionless shock waves), and fluid interfaces in the atmosphere (Smith 1988; Christie 1992; Rottman and Grimshaw 2001) and ocean (Holloway et al. 2001).

The Whitham averaging technique Whitham (1965, 1974) is a principal analytical tool for dispersive regularization of singularity formation in hyperbolic systems; see, e.g., the review (Hoefer and Ablowitz 2009). The method is used to describe slow modulations of a nonlinear, periodic traveling wave. Given an $n$th-order nonlinear evolution equation, implementation of the method requires the existence of an $n$-parameter family of periodic traveling wave solutions $\phi(\xi; \mathbf{p}), \mathbf{p} \in \mathbb{R}^n$ with period $L = L(\mathbf{p})$, coordinate $\xi = x - ct$, and speed $c = c(\mathbf{p})$. Additionally, the evolution equation must admit $n - 1$ conserved densities $\mathcal{P}_i[\phi]$ and fluxes $\mathcal{Q}_i[\phi]$, $i = 1, 2, \ldots, n - 1$ corresponding to the conservation laws

$$\frac{\partial}{\partial t}\mathcal{P}_i + \frac{\partial}{\partial x}\mathcal{Q}_i = 0, \qquad i = 1, \ldots, n - 1. \tag{1.1}$$

Assuming slow spatiotemporal evolution of the wave's parameters $\mathbf{p}$, the conservation laws are then averaged over a period, resulting in the modulation equations

$$\left(\frac{1}{L}\int_0^L \mathcal{P}_i[\phi(\xi; \mathbf{p})]\mathrm{d}\xi\right)_t + \left(\frac{1}{L}\int_0^L \mathcal{Q}_i[\phi(\xi; \mathbf{p})]\mathrm{d}\xi\right)_x = 0, \qquad i = 1, \ldots, n - 1. \tag{1.2}$$

The $n$ Whitham modulation equations are completed by the addition of the conservation of waves to (1.2)

$$k_t + \omega_x = 0, \quad k = 2\pi/L, \quad \omega = kc, \tag{1.3}$$

a consistency condition for the application of modulation theory. The Whitham equations are a set of first-order, quasilinear partial differential equations (PDEs) describing the slow evolution of the traveling wave's parameters $\mathbf{p}$.
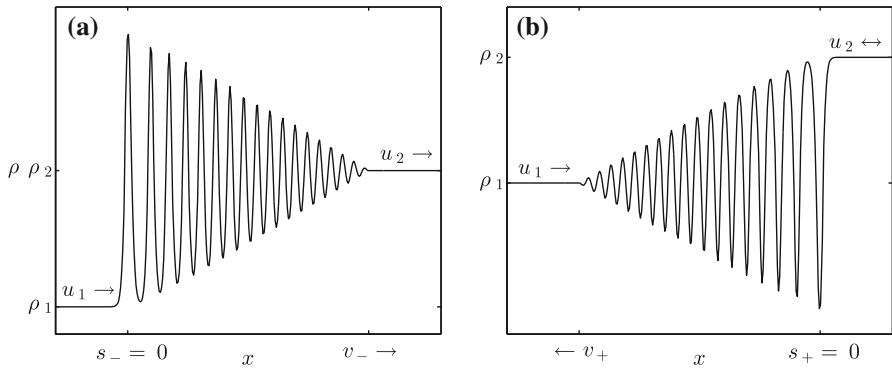
**Fig. 1** Density for the negative dispersion, $1^-$-DSW case (**a**) and positive dispersion, $1^+$-DSW case (**b**) with stationary soliton edge $s_+ = s_- = 0$ (see Sect. 6). The background flow velocities $u_1$, $u_2$ and linear wave edge velocities $v_+$, $v_-$ are also pictured. In (**a**), backflow ($v_- < 0$) occurs, while in (**b**), it is possible for the downstream flow to be negative when a vacuum point appears (see Sect. 9)

As laid out originally by Gurevich and Pitaevskii (1974), a DSW can be described by the evolution of a free boundary value problem. The boundary separates the oscillatory, one-phase region, described by the Whitham equations, from nonoscillatory, zero-phase regions, described by the dispersionless evolution equation. The regions are matched at phase boundaries by equating the average of the one-phase solution to the zero-phase solution. Thus, the free boundary is determined along with the solution. There are two ways for a one-phase wave to limit to a zero-phase solution. In the vicinity of the free boundary, either the oscillation amplitude goes to zero (harmonic limit) or the oscillation period goes to infinity, corresponding to a localization of the traveling wave (soliton limit). The determination of which limiting case to choose at a particular phase boundary requires appropriate admissibility criteria, analogous to entropy conditions for classical shock waves.

Riemann problems consisting of step initial data are an analytically tractable and physically important class to study. For a system of two genuinely nonlinear, strictly hyperbolic conservation laws, the general solution of the Riemann problem consists of three constant states connected by two self-similar waves, either a rarefaction or a shock (Lax 1973; Smoller 1994). This behavior generalizes to dispersive hydrodynamics, so borrowing terminology from classical shock theory, it is natural to label a left(right)-going wave as a 1(2)-DSW or 1(2)-rarefaction. See Fig. 1 for examples of $1^\pm$-DSWs where the $\pm$ sign corresponds to positive or negative dispersion. For a DSW resulting from the long-time evolution of step initial conditions, the oscillatory boundaries are straight lines. These leading and trailing edge speeds can be determined in terms of the left and right constant states, analogous to the Rankine–Hugoniot jump conditions of classical gas dynamics. Whitham modulation theory for DSWs was initially developed for integrable wave equations. Integrability in the context of the modulation equations (Tsarev 1985) implies the existence of a diagonalizing transformation to Riemann invariants where the Riemann problem for the hyperbolic modulation equations could be solved explicitly for a self-similar, simple wave (Gurevich and Pitaevskii 1974; Gurevich and Krylov 1987). The two DSW speeds at the

phase boundaries coinciding with the soliton and harmonic limits are the characteristic speeds of the edges of the simple wave. Thus, the dispersive regularization of breaking in a hydrodynamic system is implemented by the introduction of additional conservation laws (the Whitham equations) that admit a global solution. An important innovation was developed by El (2005) whereby the DSW's trailing and leading edge speeds could be determined without solving the full set of modulation equations. The Whitham–El DSW construction relies on the existence of a simple wave solution to the full, strictly hyperbolic and genuinely nonlinear modulation equations, but does not require its complete determination, hence analytical results are available even for nonintegrable equations.

In this work, the one-dimensional (1D) isentropic Euler equations are regularized by a class of third-order dispersive terms, modeling several of the aforementioned physical systems. The time to breaking (gradient catastrophe) for smooth initial data is numerically found to fall within bounds predicted by the dispersionless Euler equations. In order to investigate dynamics post-breaking, the long-time resolution of the Riemann problem is considered. The DSW locus relating upstream, downstream flow configurations and the DSW speeds for admissible weak shocks are determined explicitly for generic, third-order dispersive perturbations. The results depend only upon the sign of the dispersion (sgn $\omega_{kk}$) and the general pressure law assumed. A fundamental assumption in the DSW construction is the existence of an integral curve (simple wave) of the Whitham modulation equations connecting the upstream and downstream states in an averaged sense. Explicit, verifiable sufficient criteria for the breakdown of the simple wave assumption are given. The regularization for large amplitude DSWs depends upon the particular form of the dispersion. Thus, DSWs are explicitly constructed for particular pressure laws and dispersive terms of physical origin including a generalized nonlinear Schrödinger (gNLS) equation modeling superfluids and nonlinear optics. Comparisons with a dissipative regularization are presented in order to highlight the differences between viscous and dispersive shock waves.

The outline of this work is as follows. Section 2 presents the general dispersive Euler model and assumptions to be considered, followed by Sect. 3 outlining the gNLS and other dispersive Eulerian fluid models. Background Sects. 4 and 5 review the theory of the hyperbolic, dispersionless system and the Whitham–El method of DSW construction, respectively. A detailed analysis of DSW admissibility criteria and the breakdown of the simple wave assumption are undertaken in Sect. 6, followed by the complete characterization of admissible weak DSWs in Sect. 7. The theory of the breaking time for the gNLS model is shown to agree with numerical computation in Sect. 8. Large amplitude DSWs for the gNLS equation are studied in Sect. 9 both analytically and numerically. The manuscript is completed by conclusions and an appendix on the numerical methods utilized.

## 2 Dispersive Euler Equations and Assumptions

The 1D dispersive Euler equations considered in this work are, in nondimensional form,

$$\rho_t + (\rho u)_x = 0,$$
$$(\rho u)_t + \left[\rho u^2 + P(\rho)\right]_x = [D(\rho, u)]_x, \qquad -\infty < x < \infty, \qquad (2.1)$$

where $\rho$ is a fluid density, $u$ is the velocity, and $D_x$ is the (conservative) dispersive term. Formally setting $D = 0$ gives the hydrodynamic approximation, valid until gradient catastrophe when the dispersion acts to regularize the singular behavior. The dispersionless, hyperbolic, isentropic Euler equations are known as the $P$-system, whose weak solutions to the Riemann problem are well known (Wagner 1987; Smoller 1994). Here, the long-time behavior of the dispersively regularized Riemann problem is analyzed. By the formal rescaling $X = \varepsilon x, T = \varepsilon t,$

$$\rho_T + (\rho u)_X = 0,$$
$$(\rho u)_T + \left[\rho u^2 + P(\rho)\right]_X = \varepsilon^2 [D(\rho, u)]_X, \qquad -\infty < X < \infty,$$

the long-time ($t \gg 1$) behavior of the dispersive Euler equations in the independent variables $(X, T)$ is recast as a small dispersion ($\varepsilon^2 \ll 1$) problem. Due to the oscillatory nature of the small dispersion limit, it is necessarily a weak limit, as shown rigorously by Lax, Levermore, and Venakides for the Korteweg–de Vries equation (KdV) Lax and Levermore (1983a,b,c), Venakides (1985). In this work, the multiscale Whitham averaging technique will be used to study the behavior of the dispersive Euler equations (2.1) for sufficiently large time and long waves.

The Whitham–El DSW simple wave closure method El (2005) is used to construct DSWs under the following assumptions:

A1 **(sound speed)** The pressure law $P = P(\rho)$ is a smooth, monotonically increasing function of $\rho$, $P'(\rho) > 0$ for $\rho > 0$ so that the speed of sound

$$c_0 = c(\rho_0) \equiv \sqrt{P'(\rho_0)}$$

is real and the local Mach number

$$M_0 \equiv \frac{|u_0|}{c(\rho_0)}$$

is well defined. It will also be assumed that the pressure is convex, $P''(\rho) > 0$ for $\rho > 0$ so that $c'(\rho) > 0$ and ensures the genuine nonlinearity, strict hyperbolicity of the dispersionless hyperbolic system.

A2 **(symmetries)** Equations (2.1) admit the Galilean invariance

$$D(\rho, u - u_0)(x - u_0 t, t) = D(\rho, u)(x, t)$$

for all $u_0 \in \mathbb{R}$ and exhibit the sign inversion

$$D(\rho, -u)(-x, t) = -D(\rho, u)(x, t), \qquad (2.2)$$

so that (2.1) are invariant with respect to $x \to -x, u \to -u$.

A3 **(dispersive operator)** The dispersive term $[D(\rho, u)]_x$ is a differential operator with $D$ of second order in spatial and/or mixed partial derivatives such that the system (2.2) has the real-valued dispersion relation

$$\omega = u_0 k \pm \omega_0(k, \rho_0), \tag{2.3}$$

with two branches found by linearizing about the uniform background state $\rho = \rho_0$, $u = u_0$ with small amplitude waves proportional to $\exp[i(kx - \omega t)]$. The appropriate branch of the dispersion relation is fixed by the $\pm$ sign in (2.3) with $\omega_0(k, \rho_0) \geq 0$ for $k \geq 0$, $\rho_0 \geq 0$. The dispersion relation has the long-wave expansion

$$\omega_0(k, \rho_0) = c_0 k + \mu k^3 + o(k^3), \qquad k \to 0, \qquad \mu \neq 0. \tag{2.4}$$

The sign of the dispersion is $\operatorname{sgn} \omega_0''(k; \rho_0)$ for $k > 0$. Using (2.4) and the convexity or concavity of $\omega_0$ as a function of $k$, one finds

$$\operatorname{sgn}\left(\frac{\omega_0(k, \rho_0)}{k}\right)_k = \operatorname{sgn}\frac{\partial^2 \omega_0}{\partial k^2}(k, \rho_0).$$

Therefore, positive dispersion corresponds to increasing phase and group velocities with increasing $k$, while negative dispersion leads to decreasing phase and group velocities.

A4 **(Whitham averaging)** Equations (2.1) are amenable to Whitham averaging whereby a DSW can be described by a slowly varying, single-phase traveling wave. This requires:

  (i) The system possesses at least three conservation laws. The mass and momentum equations in (2.1) account for two. An additional conserved quantity is required.

 (ii) There exists a four-parameter family of periodic traveling waves parametrized by, for example, the wave amplitude $a$, the wavenumber $k$, the average density $\overline{\rho}$, and the average velocity $\overline{u}$ limiting to a trigonometric wave for small amplitude and a solitary wave for small wavenumber. In the cases considered here, the periodic traveling wave manifests as a solution of the ordinary differential equation (ODE) $(\rho')^2 = G(\rho)$, where $G$ is smooth as it varies over three simple, real roots. Two roots coincide in the small amplitude and solitary wave limits.

A5 **(Simple wave)** The Whitham–El method requires the existence of a self-similar simple wave solution to the four Whitham modulation equations (the averaged conservation laws and the conservation of waves). For this, the modulation equations must be strictly hyperbolic and genuinely nonlinear.

Assumption A1 provides for a modulationally stable, hydrodynamic long-wave limit. The symmetry assumptions in A2 are for convenience and could be neglected. As will be demonstrated in Sect. 3, A3 is a reasonable restriction still allowing for a number of physically relevant dispersive fluid models. The assumptions in A4 and A5

allow for the application of the Whitham–El method. While the assumptions in A4 are usually verifiable, A5 is often assumed. Causes of the breakdown of assumptions A3 (unique dispersion sign) and A5 (genuine nonlinearity) are identified and associated with extrema in the DSW speeds as either the left or right density is varied.

The nonstationary DSW considered here is the long-time resolution of an initial jump in the fluid density and velocity, the Riemann problem

$$u(x, 0) = \begin{cases} u_1 & x < 0 \\ u_2 & x > 0 \end{cases}, \qquad \rho(x, 0) = \begin{cases} \rho_1 & x < 0 \\ \rho_2 & x > 0 \end{cases}, \tag{2.5}$$

where $u_j \in \mathbb{R}$, $\rho_j > 0$.

## 3 Example Dispersive Fluids

The dispersive Euler equations (2.2) model a number of dispersive fluids including, among others, superfluids and optical fluids. The particular model equations described below were chosen because they incorporate different pressure laws and allow for different signs of the dispersion, key distinguishing features of Eulerian dispersive fluids and their weak dispersion regularization.

### 3.1 gNLS Equation

The generalized, defocusing nonlinear Schrödinger equation

$$\begin{aligned} i\psi_t &= -\frac{1}{2}\psi_{xx} + f(|\psi|^2)\psi, \\ f(0) &= 0, \qquad f(\rho) > 0, \qquad \rho > 0, \end{aligned} \tag{3.1}$$

or gNLS, describes a number of physical systems; For example, the "polytropic superfluid"

$$f(\rho) = \rho^p, \qquad p > 0, \tag{3.2}$$

corresponds to the cubic NLS when $p = 1$, which describes a repulsive BEC and intense laser propagation through optically defocusing (normal dispersion) media. The model (3.2) with $p = 2/3$ describes a zero-temperature Fermi gas near unitarity (Giorgini et al. 2008; Csordás et al. 2010), which is of special significance as recent experiments have been successfully interpreted with both dissipative Joseph et al. 2011 and dispersive Salasnich 2012 regularizations. Moreover, the regime $2/3 < p < 1$ describes the so-called BEC–Bardeen–Cooper–Schrieffer transition in ultracold Fermi gases (Ketterle and Zwierlein 2008). The quintic NLS case, $p = 2$, models three-body interactions in a BEC (Kevrekidis et al. 2008; Chen and Pavlovic 2011).

A BEC confined to a cigar-shaped trap exhibits effective 1D behavior that is well described by the nonpolynomial nonlinearity (Salasnich et al. 2002; Muoz Mateo and Delgado 2008)

$$f(\rho) = \frac{2\sqrt{1 + \gamma\rho} - 2}{\gamma}, \qquad \gamma > 0, \tag{3.3}$$

here scaled so that $f(\rho) \to \rho$, $\gamma \to 0^+$. In spatial nonlinear optics, photorefractive media corresponding to (Segev et al. 1992; Christodoulides and Carvalho 1995)

$$f(\rho) = \frac{\rho}{1 + \gamma\rho}, \qquad \gamma > 0 \tag{3.4}$$

are of particular interest due to recent experiments exhibiting DSWs (Wan et al. 2007; Barsi et al. 2007; Jia et al. 2007; Barsi et al. 2012; Jia et al. 2012). For $0 < \gamma \ll 1$, the leading-order behavior of (3.3) and (3.4) correspond to the cubic NLS.

The complex wavefunction $\psi$ can be interpreted in the dispersive fluid context by use of the Madelung transformation Madelung (1927)

$$\psi = \sqrt{\rho}e^{i\phi}, \qquad u = \phi_x. \tag{3.5}$$

Using (3.5) in (3.1) and equating real and imaginary parts results in the dispersive Euler equations (2.1) with

$$P(\rho) = \int_0^\rho \tilde{\rho}f'(\tilde{\rho})\mathrm{d}\tilde{\rho}, \qquad c(\rho) = \sqrt{\rho f'(\rho)},$$

$$[D(\rho, u)]_x = \frac{1}{4}\left[\rho\left(\ln\rho\right)_{xx}\right]_x = \frac{\rho}{2}\left[\frac{(\sqrt{\rho})_{xx}}{\sqrt{\rho}}\right]_x. \tag{3.6}$$

The zero dispersion limit of (2.1) corresponds to the semiclassical limit of (3.1), which in dimensional units corresponds to $\hbar \to 0$ for quantum many-body systems. In applications, the dispersive regularization coincides with a strongly interacting BEC or a large input optical intensity.

Assumption A1 restricts the admissible nonlinearity $f$ to those satisfying

$$f'(\rho) > 0, \qquad \left(\rho f'(\rho)\right)' > 0, \qquad \rho > 0, \tag{3.7}$$

which is realized by (3.2), (3.3) generally and for (3.4) when $\gamma\rho < 1$. Assumptions in A2 are well-known properties of the gNLS equation (Sulem and Sulem 1999). Assumption A3 is clear from (3.6), and the dispersion relation is

$$\omega_0(k, \rho) = k\sqrt{c^2 + k^2/4} \sim ck + \frac{1}{8c}k^3, \qquad |k| \ll c. \tag{3.8}$$

The dispersion is positive because $\omega_{0kk}(k; \rho) > 0$ for $k > 0$, $\rho > 0$.

Inserting the traveling wave ansatz

$$\rho = \rho(x - Vt), \qquad u = u(x - Vt),$$

into (2.1) with (3.6) and integrating twice leads to

$$u = V + \frac{A}{\rho}, \tag{3.9a}$$

$$(\rho')^2 = 8 \left[ \rho \int_{\rho_1}^{\rho} f(\tilde{\rho}) \mathrm{d}\tilde{\rho} + B\rho^2 + C\rho - \frac{A^2}{2} \right] \equiv G(\rho). \tag{3.9b}$$

It is assumed that $G$ has three real roots $\rho_1 \leq \rho_2 \leq \rho_3$ related to the integration constants $A$, $B$, and $C$ so that, according to a phase plane analysis, a periodic wave exists with maximum and minimum densities $\rho_2$ and $\rho_1$, respectively. The fourth arbitrary constant, due to Galilean invariance, is the wave speed $V$. In addition to mass and momentum conservation, an additional energy conservation law exists (Jin et al. 1999) which reads

$$\mathcal{E} \equiv \frac{\rho u^2}{2} + \frac{\rho_x^2}{8\rho} + \int_0^{\rho} f(\tilde{\rho}) \mathrm{d}\tilde{\rho},$$

$$\mathcal{E}_t + \{u[\mathcal{E} + P(\rho)]\}_x = \frac{1}{4} \left[ u\rho_{xx} - \frac{(\rho u)_x \rho_x}{\rho} \right]_x,$$

hence the assumptions in A4 are satisfied. The hyperbolicity of the Whitham equations can only be determined by their direct study. The genuine nonlinearity of the system will be discussed in Sect. 6. It will be helpful to note the solitary wave amplitude/speed relation which results from the boundary conditions for a depression (dark) solitary wave

$$u_0 \equiv \lim_{|\xi| \to \infty} u(\xi), \qquad \rho_0 \equiv \lim_{|x| \to \infty} \rho(\xi), \qquad \rho_{\min} \equiv \min_{\xi \in \mathbb{R}} \rho(\xi).$$

A phase plane analysis of (3.9b) implies that the roots of $G$ satisfy $\rho_1 = \rho_{\min}$, $\rho_2 = \rho_3 = \rho_0$, resulting in the solitary wave speed $s = V$ satisfying

$$(s - u_0)^2 = \frac{2\rho_{\min}}{(\rho_0 - \rho_{\min})^2} \left[ (\rho_0 - \rho_{\min}) f(\rho_0) - \int_{\rho_{\min}}^{\rho_0} f(\tilde{\rho}) \mathrm{d}\tilde{\rho} \right]. \tag{3.10}$$

The soliton profile can be determined by integration of (3.9b).

Dispersive shock waves for the gNLS equation have been studied for the pure NLS case (Gurevich et al. 1990; El and Krylov 1995) as well as in 1D photorefractive media (El et al. 2007) and the cubic–quintic case (Crosta 2011; Crosta et al. 2012). A general DSW analysis will be presented in Sect. 9.

### 3.2 Other Systems

The gNLS equation exhibits positive dispersion. Two additional examples with negative dispersion are briefly given here.

**Two-temperature collisionless plasma:** The dynamics of the ionic component of a two-temperature unmagnetized plasma (Karpman 1974) satisfy the dispersive Euler equations with

$$P(\rho) = \rho, \qquad c(\rho) = 1,$$
$$D(\rho, u) = \frac{1}{2}\phi_x^2 - \phi_{xx}, \qquad -\phi_{xx} + e^\phi = \rho.$$

The electronic potential $\phi$ introduces nonlocal dispersion with dispersion relation

$$\omega_0(k, \rho) = \frac{k}{\sqrt{1 + k^2/\rho}} \sim k - \frac{k^3}{2\rho_0}, \qquad |k| \ll 1.$$

It can be shown that $\omega_{kk} < 0, k > 0$, thus the system exhibits negative dispersion.

This system has been analyzed in detail Gurevich et al. (1990) and satisfies assumptions A1–A4. Large amplitude dispersive shock waves were constructed in El (2005) under the assumptions of A5.

**Fully nonlinear shallow water:** Shallow waves in an ideal fluid with no restriction on amplitude satisfy the generalized Serre equations (also referred to as the Su–Gardner or Green–Naghdi equations) (Serre 1953; Su and Gardner 1969; Green and Naghdi 1976; Dias and Milewski 2010) with

$$P(\rho) = \frac{1}{2}\rho^2, \qquad c(\rho) = \sqrt{\rho},$$
$$D(\rho, u) = \frac{1}{3}\left[\rho^3\left(u_{tx} + uu_{xx} - u_x^2\right)\right] + \sigma\left(\rho\rho_{xx} - \frac{1}{2}\rho_x^2\right). \qquad (3.11)$$

The density $\rho$ corresponds to the free surface fluid height, and $u$ is the vertically averaged horizontal fluid velocity. The Bond number $\sigma \geq 0$ is proportional to the coefficient of surface tension. The dispersion relation is

$$\omega_0(k, \rho) = k\left(\rho\frac{1 + \sigma k^2}{1 + \rho^2 k^2/3}\right)^{1/2}$$
$$\sim \sqrt{\rho}\left(k + \frac{3\sigma - \rho^2}{6}k^3\right), \qquad k \to 0.$$

The sign of the dispersion changes when $\omega_{kk} = 0$, corresponding to the critical values

$$\sigma_{\text{cr}} = \frac{\rho^2}{3} \quad \text{or} \quad k_{\text{cr}} = \frac{1}{\rho}\left(3 + 3\sqrt{1 + \rho^2/\sigma}\right)^{1/2}.$$

The critical value $\sigma_{\text{cr}}$ expresses the fact that shallow water waves with weak surface tension effects, $\sigma < \sigma_{\text{cr}}$, exhibit negative dispersion for sufficiently long waves ($k < k_{\text{cr}}$)

and support elevation solitary wave solutions. Strong surface tension, $\sigma > \sigma_{cr}$, corresponds to positive dispersion and can yield depression solitary waves. Assumptions A1–A4 hold (Dias and Milewski 2010). DSWs in the case of zero surface tension $\sigma = 0$ were studied in El et al. (2006).

It is worth mentioning that the Serre equations (3.11) with $\sigma = 0$ and a model of liquid containing small gas bubbles (Wijngaarden 1972) can be cast in Lagrangian form to fit into the framework of "continua with memory" (Gavrilyuk. and Teshukov 2001). The Whitham modulation equations for these dispersive Eulerian fluids were studied in Gavrilyuk (1994). Explicit, sufficient conditions for hyperbolicity of the modulation equations were derived.

The properties of DSWs for these systems will be discussed briefly in Sect. 10.

## 4 Background: Dispersionless Limit

The analysis of DSWs for (2.1) requires an understanding of the dispersionless limit

$$
\begin{aligned}
\rho_t + (\rho u)_x &= 0, \\
(\rho u)_t + \left[\rho u^2 + P(\rho)\right]_x &= 0,
\end{aligned}
\tag{4.1}
$$

corresponding to $D \equiv 0$. Equations (4.1) are the equations of compressible, isentropic gas dynamics with pressure law $P(\rho)$ (Liepmann and Roshko 1957). They are hyperbolic and diagonalized by the Riemann invariants (see, e.g., Courant and Friedrichs 1948)

$$
r_1 = u - \int^{\rho} \frac{c(\rho')}{\rho'}\mathrm{d}\rho', \qquad r_2 = u + \int^{\rho} \frac{c(\rho')}{\rho'}\mathrm{d}\rho',
\tag{4.2}
$$

with the characteristic velocities

$$
\lambda_1 = u - c(\rho), \qquad \lambda_2 = u + c(\rho),
\tag{4.3}
$$

so that

$$
\frac{\partial r_j}{\partial t} + \lambda_j \frac{\partial r_j}{\partial x} = 0, \qquad j = 1, 2.
\tag{4.4}
$$

By monotonicity of

$$
g(\rho) = \int^{\rho} \frac{c(\rho')}{\rho'}\mathrm{d}\rho',
$$

the inversion of (4.2) is achieved via

$$
u = \frac{1}{2}(r_1 + r_2), \qquad \rho = g^{-1}\left(\frac{1}{2}(r_2 - r_1)\right).
\tag{4.5}
$$

In what follows, an overview of the properties of equations (4.1) is provided for both the required analysis of DSWs and for the comparison of classical and dispersive shock waves.

## 4.1 Breaking Time

Smooth initial data may develop a singularity in finite time. The existence of Riemann invariants (4.2) allows for estimates of the breaking time at which this occurs. In what follows, Lax's breaking time estimates Lax (1964) are applied to the system (4.4) with smooth initial data.

Lax's general approach for $2 \times 2$ hyperbolic systems is to reduce the Riemann invariant system (4.4) to the equation

$$z' = -a(t)z^2, \qquad z(0) = m, \tag{4.6}$$

along a characteristic family, $' \equiv \frac{\partial}{\partial t} + \lambda_i \frac{\partial}{\partial x}$, and then bound the breaking time by comparison with an autonomous equation via estimates for $a$ and $m$ in terms of initial data for $r_1, r_2$.

Following Lax (1964), integration along the 1-characteristic family in (4.6) leads to $z = e^h \partial r_1 / \partial x$, $a = e^{-h} \partial \lambda_1 / \partial r_1$ and $h(r_1, r_2)$ satisfies

$$\frac{\partial h}{\partial r_2} = \frac{\frac{\partial \lambda_1}{\partial r_2}}{\lambda_1 - \lambda_2}.$$

By direct computation with Eqs. (4.2), (4.3), one can verify the following:

$$h = \frac{1}{2} \ln \left[ \frac{c(\rho)}{\rho} \right], \tag{4.7a}$$

$$a = e^{-h} \frac{\partial \lambda_1}{\partial r_1} = \frac{c(\rho) + \rho c'(\rho)}{2c(\rho)} \left[ \frac{\rho}{c(\rho)} \right]^{1/2}, \tag{4.7b}$$

$$z = e^h \frac{\partial r_1}{\partial x} = \frac{\partial r_1}{\partial x} \left[ \frac{c(\rho)}{\rho} \right]^{1/2}. \tag{4.7c}$$

The initial data for $r_1$ and $r_2$ are assumed to be smooth and bounded so that they satisfy

$$\underline{r_1} \le r_1(x, t) \le \overline{r_1}, \qquad \underline{r_2} \le r_2(x, t) \le \overline{r_2}, \qquad 0 \le t < t_{br}. \tag{4.8}$$

Assuming $\rho > 0$ (nonvacuum conditions), then (4.7b) implies $a > 0$ and $z$ is decreasing along the 1-characteristic. Bounds for $a(t)$ are defined as follows:

$$A = \min_{\rho \in R_A} a, \qquad B = \max_{\rho \in R_B} a, \tag{4.9}$$

where $R_A$ and $R_B$ are intervals related to the bounds on the initial data, chosen shortly. The initial condition $m$ is chosen as negative as possible

$$x_0 = \arg\min_{x \in \mathbb{R}} z(0) = \arg\min_{x \in \mathbb{R}} \left[ \frac{\partial u}{\partial x} - \frac{c(\rho)}{\rho} \frac{\partial \rho}{\partial x} \right] \left[ \frac{c(\rho)}{\rho} \right]^{1/2} \Bigg|_{t=0}, \tag{4.10a}$$

$$m = \min_{x \in \mathbb{R}} z(0) = \left[ \frac{\partial u}{\partial x} - \frac{c(\rho)}{\rho} \frac{\partial \rho}{\partial x} \right] \left[ \frac{c(\rho)}{\rho} \right]^{1/2} \Bigg|_{(x,t)=(x_0,0)}. \tag{4.10b}$$

These estimates lead to the following bounds on the breaking time $t_{\mathrm{br}}$:

$$-\frac{1}{mB} \le t_{\mathrm{br}} \le -\frac{1}{mA}. \tag{4.11}$$

It is still necessary to provide the intervals $R_A$ and $R_B$. The possible values of $r_1$ and $r_2$ in (4.8) and the monotonicity of the transformation for $\rho$ in (4.5) suggest taking the full range of possible values $R_A = R_B = [g^{-1}((\underline{r_2} - \overline{r_1})/2), g^{-1}((\overline{r_2} - \underline{r_1})/2)]$. However, this choice does not provide the sharpest estimates in (4.11). The idea is to use the fact that $r_1$ is constant along 1-characteristics. The choice for $m$ in (4.10b) suggests taking $r_1 = r_1(x_0, 0)$ and allowing $r_2$ to vary across its range of values. While the optimal $m$ is associated with this characteristic, it does not necessarily provide the optimal estimates for $A$ or $B$. A calculation shows

$$\frac{\partial a}{\partial r_1} = -\frac{1}{8c^3} \left( \frac{\rho}{c} \right)^{1/2} \left( c^2 - 4\rho cc' - 2\rho^2 cc'' + 3\rho^2 c'^2 \right).$$

It can be verified that $\partial a / \partial r_1 \le 0$ for the example dispersive fluids considered here. In this case, any characteristic with $r_1 < r_1(x_0, 0)$ can cause $a$ to *increase*, leading to a larger $A$ and a tighter bound in (4.11). If $r_1 > r_1(x_0, 0)$, then $a$ may *decrease*, leading to a smaller $B$ and a tighter bound on $t_{\mathrm{br}}$. Combining these deductions leads to the choices

$$R_A = \left[ g^{-1} \left( \frac{\underline{r_2} - r_1(x_0, 0)}{2} \right), g^{-1} \left( \frac{\overline{r_2} - \underline{r_1}}{2} \right) \right], \tag{4.12a}$$

$$R_B = \left[ g^{-1} \left( \frac{\underline{r_2} - \overline{r_1}}{2} \right), g^{-1} \left( \frac{\overline{r_2} - r_1(x_0, 0)}{2} \right) \right], \tag{4.12b}$$

when $\partial a / \partial r_1 < 0$.

In summary, given initial data satisfying (4.8), the point $x_0$ and $m$ are determined from (4.10a) and (4.10b). If $m > 0$, then there is no breaking. Otherwise, after verifying $\partial a / \partial r_1 < 0$, the sets $R_A$ and $R_B$ are defined via (4.12a) and (4.12b), leading to $A$ and $B$ in (4.9). The breaking time bounds are given by (4.11). A similar argument integrating along the 2-characteristic field yields another estimate for the breaking time $t_{\mathrm{br}}$. The only changes are in (4.10a) and (4.10b), where the minus sign goes to a plus sign and the choices for $R_A$ and $R_B$ reflect $r_2(x_0, 0)$. These results will be used to estimate breaking times for dispersive fluids in Sect. 8, demonstrating the validity of the hydraulic approximation, hence the equivalence of dispersive and dissipative regularizations up to breaking.

### 4.2 Viscous Shock Waves

It will be interesting to contrast the behavior of dispersive shock waves for (2.1) with that of classical, viscous shock waves resulting from a dissipative regularization of the dispersionless equations. For this, the jump and entropy conditions for shocks are summarized below Courant and Friedrichs (1948), Smoller (1994).

The Riemann problem (2.5) for (4.1) results in the Hugoniot loci of classical shock solutions

$$u_2 = u_1 \pm \left\{ \frac{[P(\rho_2) - P(\rho_1)](\rho_2 - \rho_1)}{\rho_1 \rho_2} \right\}^{1/2}. \tag{4.13}$$

The $-$ $(+)$ sign corresponds to an admissible 1-shock (2-shock) satisfying the Lax entropy conditions when the characteristic velocity $\lambda_1$ ($\lambda_2$) *decreases* across the shock so that $\rho_2 > \rho_1 > 0$ ($\rho_1 > \rho_2 > 0$). Weak 1-shocks connecting the densities $\rho_1$ and $\rho_2 = \rho_1 + \Delta, 0 < \Delta \ll \rho_1$ exhibit the shock speed

$$v^{(1)} \sim u_1 - c_1 - \frac{1}{2} \left( \frac{c_1}{\rho_1} + c_1' \right) \Delta, \qquad 0 < \Delta \ll \rho_1. \tag{4.14}$$

While the Riemann invariant $r_2$ exhibits a jump across the 1-shock, it is third order in $\Delta / \rho_1$ so is approximately conserved for weak shocks. Weak, steady (nonpropagating) 1-shocks satisfy the jump conditions

$$\Delta \sim \frac{2\rho_1 c_1}{c_1 + \rho_1 c_1'}(M_1 - 1),$$
$$M_2 \sim 1 - (M_1 - 1), \qquad 0 < M_1 - 1 \ll 1, \tag{4.15}$$

where $M_j = |u_j|/c_j$ are the Mach numbers of the up/downstream flows and $c_1' \equiv \frac{dc}{d\rho}(\rho_1)$. The upstream flow indexed by 1 is supersonic and the downstream flow is subsonic, this behavior also holding for arbitrary amplitude shocks.

### 4.3 Rarefaction Waves

Centered rarefaction wave solutions of (4.1) exhibit the following wave curves connecting the left and right states:

$$1 - \text{rarefaction}: \quad u_1 = u_2 + \int_{\rho_1}^{\rho_2} \frac{c(\rho)}{\rho} \, d\rho, \qquad \rho_1 > \rho_2, \qquad (4.16a)$$

$$2 - \text{rarefaction}: \quad u_1 = u_2 - \int_{\rho_1}^{\rho_2} \frac{c(\rho)}{\rho} \, d\rho, \qquad \rho_2 > \rho_1, \qquad (4.16b)$$

where admissibility is opposite to the shock wave case. The characteristic velocities $\lambda_j$ *increase* across a rarefaction wave. Since rarefaction waves are continuous and do not involve breaking, the leading-order behavior of dispersive and dissipative regularizations for (4.1) are the same. A dispersive regularization of KdV (Novikov et al. 1984; Leach and Needham 2008) shows the development of small amplitude oscillations for the first-order singularities at either the left or right edge of the rarefaction wave, with one decaying as $\mathcal{O}(t^{-1/2})$ and the other $\mathcal{O}(t^{-2/3})$. The width of these oscillations expands as $\mathcal{O}(t^{1/3})$ (Gurevich and Pitaevskii 1974), so that their extent vanishes relative to the rarefaction wave expansion with $\mathcal{O}(t)$.

### 4.4 Shock Tube Problem

Recall that the general solution of the Riemann problem consists of three constant states connected by two waves, each either a rarefaction or shock (Lax 1973; Smoller 1994). The shock tube problem (Liepmann and Roshko 1957) involves a jump in density for a quiescent fluid $u_1 = u_2 = 0$. The solution consists of a shock and rarefaction connected by a constant, intermediate state $(\rho_m, u_m)$. For the case $\rho_1 < \rho_2$, a 1-shock connects to a 2-rarefaction via the Hugoniot locus (4.13) (with $-$) and the wave curve (4.16b), respectively. For example, a polytropic gas with $P(\rho) = \kappa \rho^\gamma$ gives the two equations

$$1 - \text{shock}: \quad u_m = -\left[ \frac{(\kappa \rho_m^\gamma - \kappa \rho_1^\gamma)(\rho_m - \rho_1)}{\rho_m \rho_1} \right]^{1/2},$$

$$2 - \text{rarefaction}: \quad u_m = -\frac{2(\kappa \gamma)^{1/2}}{\gamma - 3} \left[ \rho_2^{(\gamma-1)/2} - \rho_m^{(\gamma-1)/2} \right]. \qquad (4.17)$$

Equating these two expressions provides an equation for the intermediate density $\rho_m$, and then the intermediate velocity $u_m$ follows.

## 5 Background: Simple DSWs

The long-time behavior of a DSW for the dispersive Euler model (2.1) was first considered in El (2005). In this section, the general Whitham–El construction of a simple wave led DSW for step initial data is reviewed. This introduces necessary notation and background that will be used in the later sections of this work.

Analogous to the terminology for classical shocks, a 1-DSW is associated with the $\lambda_1$ characteristic family of the dispersionless system (4.1) involving left-going waves. In this case, the DSW leading edge is defined to be the leftmost (most negative) edge whereas the DSW trailing edge is the rightmost edge, these roles being reversed for the 2-DSW associated with the $\lambda_2$ characteristic family. There is a notion of polarity associated with a DSW corresponding to its limiting behavior at the leading and trailing edges. The edge where the amplitude of the DSW oscillations vanishes (the harmonic limit) is called the linear wave edge. The soliton edge is associated with the phase boundary where the DSW wavenumber $k \to 0$ (the soliton limit). Thus, the soliton edge could be the leading or trailing edge of the DSW, each case corresponding to a different DSW polarity. The polarity is generally determined by admissibility criteria and typically follows directly from the sign of the dispersion (Gurevich et al. 1990), as will be shown in Sect. 6. The DSW construction for 1-DSWs is outlined below. A similar procedure holds for 2-DSWs.

Assuming the existence of a DSW oscillatory region described by slow modulations of the periodic traveling wave from assumption A4, three independent conservation laws are averaged with the periodic wave. The wave's parameters ($\overline{\rho}$, the average density; $\overline{u}$, the average velocity; $k$, the generalized (nonlinear) wavenumber; and $a$, the wave amplitude) are assumed to vary slowly in space and time. The averaging procedure produces three first-order, quasilinear PDEs. This set combined with the conservation of waves, $k_t + \omega_x = 0$ ($\omega$ here is the generalized, nonlinear frequency), results in a closed system for the modulation parameters, the Whitham modulation equations. As originally formulated by Gurevich and Pitaevskii (1974), the DSW free boundary value problem is to solve the dispersionless equations (4.1) outside the oscillatory region and match this behavior to the *averaged* variables $\overline{\rho}$ and $\overline{u}$ from the Whitham equations at the interfaces with the oscillatory region where $k \to 0$ (soliton edge) or $a \to 0$ (linear wave edge). These Gurevich–Pitaevskii (GP) matching conditions correspond to the coalescence of two characteristics of the Whitham system at each edge of the DSW. Assumption A5 can be used to construct a self-similar, simple wave solution of the modulation equations connecting the $k \to 0$ soliton edge with the $a \to 0$ linear wave edge via an integral curve so that the two DSW boundaries asymptotically move with constant speed, the speeds of the double characteristics at each edge. In the Whitham–El method, the speeds are determined by the following key mathematical observations (El 2005):

- The four Whitham equations admit *exact* reductions to quasilinear systems of three equations in the $k \to 0$ (soliton edge) and $a \to 0$ (linear wave edge) regimes.
- Assuming a simple wave solution of the *full* Whitham equations, one can integrate across the DSW with explicit knowledge only of the reduced systems in the $a = 0$ or $k = 0$ plane of parameters, thereby obtaining the DSW leading and trailing edge speeds.

This DSW closure method is appealing because it bypasses the difficult determination and solution of the full Whitham equations. Furthermore, it applies to a large class of nonintegrable nonlinear wave equations. Some nonintegrable equations studied with this method include dispersive Euler equations for ion-acoustic plasmas (El 2005), the Serre equations with zero surface tension (El et al. 2006), the gNLS equation with

photorefractive (El et al. 2007) and cubic/quintic nonlinearity (Crosta et al. 2012), and other equations including the Miyata–Camassa–Choi equations of two-layer fluids (Esler and Pearce 2011).

Simple DSWs are described by a simple wave solution of the Whitham modulation system which necessitates self-similar variation in only one characteristic field. Using a nontrivial backward characteristic argument, it has been shown that a simple wave solution requires the constancy of one of the Riemann invariants (4.2) evaluated at the left and right states (El 2005). Then a necessary condition for a simple DSW is one of

$$1 - \text{DSW}: \quad u_2 = u_1 - \int_{\rho_1}^{\rho_2} \frac{c(\rho)}{\rho} d\rho, \qquad \rho_2 > \rho_1, \tag{5.1}$$

$$2 - \text{DSW}: \quad u_2 = u_1 + \int_{\rho_1}^{\rho_2} \frac{c(\rho)}{\rho} d\rho, \qquad \rho_1 > \rho_2. \tag{5.2}$$

1-DSWs (2-DSWs) are associated with constant $r_2$ ($r_1$) hence vary in the $\lambda_1$ ($\lambda_2$) characteristic field. Equations (5.1), (5.2) can be termed *DSW loci* as they are the dispersive shock analogs of the Hugoniot loci (4.13) for classical shock waves. It is worth pointing out that the DSW loci correspond precisely to the rarefaction wave curves in (4.16a) and (4.16b). However, the admissibility criteria for DSWs correspond to *inadmissible*, compressive rarefaction waves where the dispersionless characteristic speed decreases across the DSW. Coincidence of rarefaction and shock curves does occur in classical hyperbolic systems but is restricted to a specific class, the so-called *Temple systems* Temple (1983) to which the dispersionless Euler equations do not belong.

Recall from Sect. 4.2 that, across a viscous shock, a Riemann invariant is conserved to third order in the jump height. Since the DSW loci (5.1), (5.2) result from a constant Riemann invariant across the DSW, the DSW loci are equal to the Hugoniot loci (4.13) up to third order in the jump height.

### 5.1 Linear Wave Edge

The integral curve of the Whitham equations in the $a = 0$ (linear wave edge) plane of parameters reduces to the relationships $k = k(\overline{\rho})$, $\overline{u} = \overline{u}(\overline{\rho})$ and the ODE

$$\frac{dk}{d\overline{\rho}} = \frac{\omega_{\overline{\rho}}}{\overline{u}(\overline{\rho}) - c(\overline{\rho}) - \omega_k}, \tag{5.3}$$

where the average velocity is constrained by the density through a generalization of (5.1)

$$\overline{u}(\overline{\rho}) = u_1 - \int_{\rho_1}^{\overline{\rho}} \frac{c(\rho')}{\rho'} d\rho'. \tag{5.4}$$

The negative branch of the linear dispersion relation in (2.3), $\omega = \overline{u}(\overline{\rho})k - \omega_0(k, \overline{\rho})$, is associated with left-going waves, hence a 1-DSW.

Using (5.4) and (2.3), (5.3) simplifies to

$$\frac{\mathrm{d}k}{\mathrm{d}\overline{\rho}} = \frac{ck/\overline{\rho} + \omega_{0\overline{\rho}}}{c - \omega_{0k}}. \tag{5.5}$$

Equation (5.5) assumes $a = 0$, an exact reduction of the Whitham equations only at the linear wave edge. Global information associated with the simple wave solution of the full Whitham equations is obtained from the GP matching condition at the soliton edge by noting that the modulation variables satisfy $(k, \overline{\rho}, \overline{u}, a) = (0, \rho_j, u_j, a_j)$ for some $j \in \{1, 2\}$ depending on whether the soliton edge is leading or trailing, *independent* of the soliton amplitude $a_j$. Thus, (5.5) can be integrated in the $a = 0$ plane with the initial condition $k(\rho_j) = 0, \overline{u}(\rho_j) = u_j$ to $k(\rho_{3-j})$ associated with the linear wave edge, giving the wavenumber of the linear wave edge oscillations. This wavepacket's speed is then determined from the group velocity $\omega_k$.

Based on the Riemann data (2.5), the integration domain for (5.5) is $\overline{\rho} \in [\rho_1, \rho_2]$. The initial condition occurs at either the leading edge where $\overline{\rho} = \rho_1$ or the trailing edge where $\overline{\rho} = \rho_2$. The determination of the location of the linear wave edge, leading or trailing, is set by appropriate admissibility conditions discussed in Sect. 6. The solution of (5.5) with initial condition at $\rho_j$ will be denoted $k(\overline{\rho}; \rho_j)$ so that one of

$$k(\rho_j; \rho_j) = 0, \quad j = 1, 2 \tag{5.6}$$

holds for (5.5). Evaluating the solution of (5.5) at the linear wave edge $k(\rho_j; \rho_{3-j})$ gives the wavenumber of the linear wavepacket at the leading (trailing) edge when $j = 1$ ($j = 2$). The associated 1-DSW linear wave edge speed is denoted $v_j(\rho_1, \rho_2)$ and is found from the group velocity evaluated at $k(\rho_j; \rho_{3-j})$

$$\begin{aligned} v_j(\rho_1, \rho_2) &= \omega_k[k(\rho_j; \rho_{3-j}), \rho_j] \\ &= \overline{u}(\rho_j) - \omega_{0k}[k(\rho_j; \rho_{3-j}), \rho_j], \quad j = 1, 2. \end{aligned} \tag{5.7}$$

## 5.2 Soliton Edge

An exact description of the soliton edge where $k \to 0$ involves the dispersionless equations for the average density $\overline{\rho}$ and velocity $\overline{u}$ as well as an equation for the soliton amplitude $a$. While, in principle, one can carry out the simple DSW analysis on these equations, it is very convenient to introduce a new variable $\tilde{k}$ called the conjugate wavenumber. It plays the role of an amplitude and depends on $\overline{\rho}, \overline{u}$, and $a$ thus is not a new variable. The resulting modulation equations at the soliton edge then take a correspondingly symmetric form relative to the linear edge. The speed of the soliton edge is determined in an analogous way to the linear edge by introducing a conjugate frequency

$$\tilde{\omega}(\tilde{k}, \overline{\rho}) = -i\omega(i\tilde{k}, \overline{\rho}) = \overline{u}(\overline{\rho})\tilde{k} + i\omega_0(i\tilde{k}, \overline{\rho})$$
$$= \overline{u}(\overline{\rho})\tilde{k} + \tilde{\omega}_0(\tilde{k}, \overline{\rho}). \tag{5.8}$$

The conjugate wavenumber plays a role analogous to an amplitude so that $\tilde{k} \to 0$ corresponds to the linear wave edge where $a \to 0$. The simple wave ODE in the $k = 0$ plane is

$$\frac{d\tilde{k}}{d\overline{\rho}} = \frac{c(\overline{\rho})\tilde{k}/\overline{\rho} + \tilde{\omega}_{0_{\overline{\rho}}}}{c(\overline{\rho}) - \tilde{\omega}_{0_{\tilde{k}}}}, \tag{5.9}$$

the same equation as (5.3) but with conjugate variables. It is remarkable that the description of the soliton edge so closely parallels that of the linear wave edge. The initial condition is given at the linear wave edge where $\tilde{k} = 0$. As in (5.6), the solution with zero initial condition at $\overline{\rho} = \rho_j$ is denoted $\tilde{k}(\overline{\rho}; \rho_j)$ according to

$$\tilde{k}(\rho_j; \rho_j) = 0, \qquad j = 1, 2. \tag{5.10}$$

Then the soliton speed $s_j$, $j = 1, 2$ is the conjugate phase velocity evaluated at the conjugate wavenumber associated with the soliton edge

$$s_j(\rho_1, \rho_2) = \frac{\tilde{\omega}[\tilde{k}(\rho_j; \rho_{3-j}), \rho_j]}{\tilde{k}(\rho_j; \rho_{3-j})}$$
$$= \overline{u}(\rho_j) - \frac{\tilde{\omega}_0[\tilde{k}(\rho_j; \rho_{3-j}), \rho_j]}{\tilde{k}(\rho_j; \rho_{3-j})}. \tag{5.11}$$

*Remark 1* In a number of example dispersive fluids studied in this work and elsewhere, the transformation to the scaled phase speed

$$\alpha(\overline{\rho}) = \frac{\omega_0[k(\overline{\rho}), \overline{\rho}]}{c(\overline{\rho})k(\overline{\rho})}$$

of the dependent variable in (5.5) and the analogous transformation

$$\tilde{\alpha}(\overline{\rho}) = \frac{\tilde{\omega}_0[\tilde{k}(\overline{\rho}), \overline{\rho}]}{c(\overline{\rho})\tilde{k}(\overline{\rho})}$$

for (5.9) are helpful, reducing the ODEs (5.5) and (5.9) to simpler and, often, separable equations for $\alpha$ and $\tilde{\alpha}$.

### 5.3 Dispersive Riemann Problem

The integral wave curves (4.16a), (4.16b) and the DSW loci (5.1), (5.2) can be used to solve the dispersive Riemann problem (2.5) just as the wave curves and the Hugoniot loci are used to solve the classical Riemann problem (Smoller 1994). In both cases,
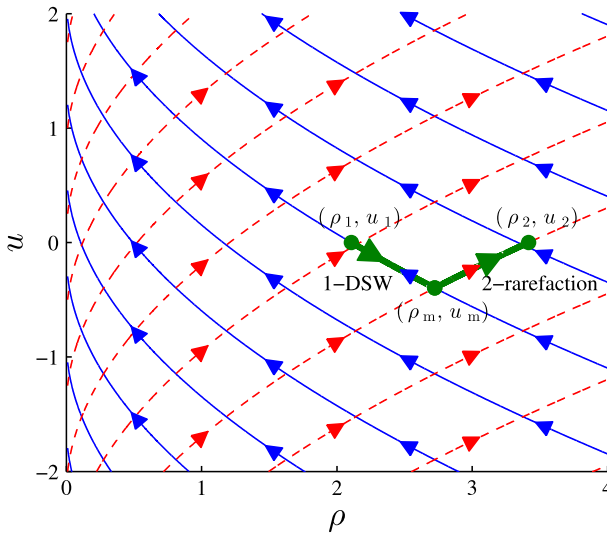
**Fig. 2** Integral curves and DSW loci for the dispersive Euler equations with $c(\rho) = \sqrt{\rho}$

the solution consists of two waves, one for each characteristic family, connected by a constant intermediate state. Each wave is either a rarefaction or a shock.

In contrast to the classical case, the integral wave curves and the DSW loci are the *same* for the dispersive Riemann problem. It is the direction in which they are traversed that determines admissibility of a rarefaction or a DSW. This enables a convenient, graphical description of solutions to the dispersive Riemann problem as shown in Fig. 2. Solid curves (——) correspond to example 1-wave curves (5.1), (4.16a), whereas dashed curves (- - - -) correspond to example 2-wave curves (5.2), (4.16b). The arrows provide the direction of increasing dispersionless characteristic speed for each wave family. Tracing an integral curve in the direction of increasing characteristic speed corresponds to an admissible rarefaction wave. The decreasing characteristic speed direction corresponds to an admissible DSW. The solution to a dispersive Riemann problem is depicted graphically by tracing appropriate integral curves to connect the left state $(\rho_1, u_1)$ with the right state $(\rho_2, u_2)$. There are multiple paths connecting these two states, but only one involves two admissible waves. This is shown by the thick curve in Fig. 2. Since the 1-wave curve is traced in the negative direction to the intermediate, constant state $(\rho_m, u_m)$, this describes a 1-DSW. The 2-wave curve is then traced in the positive direction to the right state, describing a 2-rarefaction. The 1-DSW is admissible because $\rho_m > \rho_1$. Since the characteristic speed $\lambda_2$ is monotonically increasing, the 2-rarefaction is admissible ($\rho_m < \rho_2$). The direction of the curve connecting the left and right states was taken from left to right. The opposite direction describes an inadmissible 1-rarefaction connected to an inadmissible 2-DSW.

The example shown in Fig. 2 corresponds to the dispersive shock tube problem consisting of an arbitrary jump in density for a quiescent fluid $u_1 = u_2 = 0$. Such problems have been studied in a number of dispersive fluids, e.g., El et al. (1995),

El et al. (2006), Khamis et al. (2008), Esler and Pearce (2011). The determination of $(\rho_m, u_m)$ proceeds by requiring that the left state $(\rho_1, 0)$ lie on the 1-DSW locus (5.1)

$$u_m = -\int_{\rho_1}^{\rho_m} \frac{c(\rho)}{\rho} \, d\rho. \tag{5.12}$$

The second wave connects $(\rho_m, u_m)$ to the right state $(\rho_2, 0)$ via the 2-rarefaction wave curve (4.16b)

$$u_m = -\int_{\rho_m}^{\rho_2} \frac{c(\rho)}{\rho} \, d\rho. \tag{5.13}$$

Equating (5.12) and (5.13) leads to

$$\int_{\rho_1}^{\rho_m} \frac{c(\rho)}{\rho} \, d\rho - \int_{\rho_m}^{\rho_2} \frac{c(\rho)}{\rho} \, d\rho = 0,$$

which determines the intermediate density $\rho_1 < \rho_m < \rho_2$. The intermediate velocity $u_m < 0$ follows.

This construction of the wave types and the intermediate state $(\rho_m, u_m)$ is independent of the sign of dispersion and the details of the dispersive term $D$ in (2.1), depending only upon the pressure law $P(\rho)$. For example, polytropic dispersive fluids with $P(\rho) = \kappa \rho^\gamma$ [e.g., gNLS with power-law nonlinearity (3.2) and gSerre (3.11)] yield the intermediate state (previously presented in Gurevich and Meshcherkin 1984)

$$\rho_m = \left[ \frac{1}{2} \left( \rho_1^{(\gamma-1)/2} + \rho_2^{(\gamma-1)/2} \right) \right]^{2/(\gamma-1)},$$

$$u_m = \frac{2(\kappa\gamma)^{1/2}}{3-\gamma} \left[ \rho_1^{(\gamma-1)/2} - \rho_2^{(\gamma-1)/2} \right]. \tag{5.14}$$

This prediction will be compared with numerical computations of gNLS in Sect. 9.2.

## 6 DSW Admissibility Criteria

As shown in Sect. 4.3, when (5.1) holds and $\rho_1 > \rho_2$, a continuous 1-rarefaction wave solution to the dispersionless equations exists. Gradient catastrophe does not occur, so the rarefaction wave correctly captures the leading-order behavior of the dispersive regularization. However, when $\rho_1 < \rho_2$, the rarefaction wave solution is no longer admissible and integrating the dispersionless equations via the method of characteristics results in a multivalued solution. A dispersive regularization leading to a DSW is necessitated. Specific criteria are now provided to identify admissible 1-DSWs.

The general admissibility criteria for DSWs depend on the ordering of the soliton and linear wave edges. In what is termed here a "$1^+$-DSW," the conditions are El (2005)

$$u_2 - c_2 < s_2 < u_2 + c_2, \tag{6.1a}$$

$$1^+-\text{DSW}: \quad v_1 < u_1 - c_1, \tag{6.1b}$$

$$s_2 > v_1, \tag{6.1c}$$

where the soliton is at the *trailing* edge of the DSW. Similarly, a "$1^-$-DSW" satisfies the conditions

$$u_2 - c_2 < v_2 < u_2 + c_2, \tag{6.2a}$$

$$1^--\text{DSW}: \quad s_1 < u_1 - c_1, \tag{6.2b}$$

$$v_2 > s_1, \tag{6.2c}$$

with the soliton at the *leading* edge. The designation $1^+$-DSW ($1^-$-DSW) corresponds to a positive (negative) dispersion fluid, as shown below. Recall that the soliton (linear) edge speed $s_j$ ($v_j$) corresponds to the left edge of the DSW if $j = 1$ or the right edge if $j = 2$. Thus, the subscript determines the polarity of the DSW. These conditions are analogous to the Lax entropy conditions for dissipatively regularized hyperbolic systems Lax (1973). A key difference from classical fluids is that there is only one "sign" of dissipation due to time irreversibility; for time-reversible, dispersive fluids, both signs are possible. The admissibility criteria ensure that only three characteristics impinge upon the three-parameter DSW, transferring initial/boundary data into the DSW and allowing for the simple wave condition (5.1) to hold. Sufficient conditions for these criteria as applied to the dispersive Euler equations are now shown.

First, consider the criteria for a $1^+$-DSW in a positive dispersion fluid. Inserting the linear wave and soliton edge speeds (5.7), (5.11) into inequalities (6.1a), (6.1b) simplifies the first two admissibility criteria to

$$-c_2 < \frac{\tilde{\omega}_0(\tilde{k}_2, \rho_2)}{\tilde{k}_2} < c_2, \tag{6.3a}$$

$$\omega_{0_k}(k_1, \rho_1) > c_1, \tag{6.3b}$$

where $\tilde{k}_2 = \tilde{k}(\rho_2; \rho_1)$ and $k_1 = k(\rho_1; \rho_2)$. In Sect. 7.3, the admissibility of weak $1^+$-DSWs when $0 < \rho_2 - \rho_1 \ll 1$ is demonstrated. The further assumptions

$$1^+-\text{DSW}: \quad \tilde{\omega}_{\tilde{k}\tilde{k}} < 0, \quad ck + \overline{\rho}\omega_{0_{\overline{\rho}}} > 0, \quad c\tilde{k} + \overline{\rho}\tilde{\omega}_{0_{\overline{\rho}}} > 0 \tag{6.4}$$

enable the extrapolation of Eulerian $1^+$-DSW admissibility to moderate and large jumps $\rho_2 > \rho_1$ (below). Assumptions (6.4) hold for gNLS, gSerre, and ion-acoustic plasma in certain parameter regimes (moderate jumps).

The extrapolation of admissibility to larger jumps can be demonstrated as follows. For 1-DSWs, the negative branch of the dispersion relation (2.3) has been chosen for $k > 0$. Using the small $k$ asymptotics (2.4) in (5.5) with initial condition $k(\rho_2; \rho_2) = 0$, one can show that $k(\overline{\rho}; \rho_2)$ is a decreasing function of $\overline{\rho}$ for $|\overline{\rho} - \rho_2| \ll \rho_2$. Since $\omega_{0_k}(0, \overline{\rho}) = c(\overline{\rho})$, the convexity of $\omega_0$ implies $\omega_{0_k}(k, \overline{\rho}) > c(\overline{\rho})$ for $k > 0$. This fact combined with (6.4) in (5.5) implies that $k_1 = k(\rho_1; \rho_2) > 0$ for $\rho_2 > \rho_1$ and that inequality (6.3b) holds. Similar arguments demonstrate that $\tilde{k}_2 = \tilde{k}(\rho_2; \rho_1) > 0$ for $\rho_2 > \rho_1$ and that the inequalities in (6.3a) hold. Thus, if (6.4) hold for an interval $k \in [0, k_*)$, then (6.3a) and (6.3b) are verified for $\rho_2 \in (\rho_1, \rho_*)$ where $k(\rho_1; \rho_*) = k_*$. It is now clear why $\rho_2 > \rho_1$ in (5.1) and the designation $1^+$-DSW is used when the sign of dispersion is positive.

By similar arguments, inequalities (6.2a) and (6.2b) hold for negative dispersion fluids when $\rho_1 < \rho_2$ and

$$1^- - \text{DSW}: \quad \tilde{\omega}_{\tilde{k}\tilde{k}} > 0, \quad ck + \overline{\rho}\omega_{0_{\overline{\rho}}} > 0, \quad c\tilde{k} + \overline{\rho}\tilde{\omega}_{0_{\overline{\rho}}} > 0. \quad (6.5)$$

The only change with respect to (6.4) is the convexity of the conjugate dispersion relation.

The final inequalities (6.1c) and (6.2c) require verification. An explicit analysis for weak DSWs is given in Sect. 7. An intuitive argument can be given for the general case. When $\omega_{kk} > 0$, the case of positive dispersion, the group velocity of waves with shorter wavelengths is larger, while the opposite is true for negative dispersion. The soliton edge corresponds to the longest wavelength (infinite) hence should be the trailing (leading) edge in positive (negative) dispersion systems. For the 1-DSW, a trailing soliton edge means $s > v$ as is the case in (6.1c). A leading soliton edge corresponds to the ordering in (6.2c).

In summary, sufficient conditions for a simple wave led 1-DSW are $\rho_1 < \rho_2$ and either (6.1c), (6.4) for a positive dispersion $1^+$-DSW or (6.2c), (6.5) for a negative dispersion $1^-$-DSW. Because of this, it is convenient to dispense with the subscripts defining the DSW speeds $v_j$ and $s_j$ in (5.7), (5.11) and use the notation

$$v_- \equiv v_2, \quad v_+ \equiv v_1, \quad s_- \equiv s_1, \quad s_+ \equiv s_2, \quad (6.6)$$

which identifies the dispersion sign. The conditions (6.4) or (6.5) can be verified a priori, while the speed orderings (6.1c) or (6.2c) must be verified by computing the speeds directly. For the case of $2^\pm$-DSWs, the requirement is $\rho_1 > \rho_2$ and the appropriate ordering of the soliton and linear wave edges. The Lax entropy conditions for the dissipative regularization of the Euler equations give similar criteria, namely positive (negative) jumps for 1-shocks (2-shocks) (Smoller 1994) as is expected because dispersive and dissipative regularizations are the same up to breaking.

### 6.1 Nonstationary and Stationary Soliton Edge

Due to Galilean invariance, there is flexibility in the choice of reference frame for the study of DSWs. In the general construction of 1-DSWs presented here, the laboratory

frame was used with the requirement that the background flow variables lie on the 1-DSW locus (5.1). With this coordinate system, three of the four background flow properties ($\rho_1$, $\rho_2$, $u_1$, $u_2$) can be fixed while the fourth is determined via the 1-DSW locus. The soliton and linear wave edge speeds follow according to (5.11) and (5.7) such that either one of the admissibility criteria for a $1^+$- or $1^-$-DSW hold.

Another convenient coordinate system is one moving with the soliton edge, as shown in Fig. 1. In this case, one can consider the upstream quantities $\rho_1 > 0$, $u_1 > 0$ given and the stationary condition

$$s_\pm(\rho_1, \rho_2) = 0, \tag{6.7}$$

to hold. The downstream density $\rho_2$ is computed from (6.7), while the downstream velocity $u_2$ follows from the 1-DSW locus (5.1). The linear wave edge speed is found, as usual, from (5.7).

The admissibility criteria (6.1a)–(6.2c) for a 1-DSW with stationary soliton edge become

$$1^+\text{–DSW}: \quad M_2 - 1 < 0 < M_2 + 1, \quad \frac{v_1}{c_1} < M_1 - 1, \quad v_1 < 0,$$

$$1^-\text{–DSW}: \quad M_2 - 1 < \frac{v_2}{c_2} < M_2 + 1, \quad 1 < M_1, \quad v_2 > 0.$$

For $1^+$-DSWs, the downstream flow must be subsonic ($M_2 < 1$), while for $1^-$-DSWs, the upstream flow must be supersonic ($M_1 > 1$). It is expected that both properties hold for both $1^\pm$-DSWs, but this is not required by the admissibility criteria. Supersonic upstream flow and subsonic downstream flow is consistent with classical shock waves and will be demonstrated for weak DSWs in Sect. 7.

The DSW locus (5.1), the linear wave edge speed in (5.7), and the soliton edge speed in (5.11) along with the stationary condition (6.7) constitute the jump conditions for a 1-DSW with a stationary soliton edge in dispersive Eulerian fluids. Given the upstream Mach number $M_1$ and density $\rho_1$, the stationary condition (6.7) and the soliton edge speeds (5.11) determine the downstream density $\rho_2$ while the DSW locus (5.1) determines the downstream Mach number $M_2$.

Figure 1 depicts generic descriptions of $1^\pm$-DSWs with stationary soliton edge. In the $1^-$-DSW case of Fig. 1a, the soliton edge is the leading edge and the linear wave edge is the trailing edge. The opposite orientation is true for the $1^+$-DSW shown in Fig. 1b. This behavior was also depicted in Gurevich et al. (1990) based on an analysis of weak DSWs in plasma.

## 6.2 Breakdown of Simple Wave Assumption

A fundamental assumption in this DSW construction is the existence of a simple wave or integral curve of the full Whitham modulation equations connecting the trailing and leading edge states. This assumption is in addition to the admissibility criteria discussed in this Section. The simple wave assumption for a 1-DSW requires a monotonic decrease of the associated characteristic speed as the integral curve is traversed from

left to right (Dafermos 2009). This monotonicity condition leads to the requirement of genuine nonlinearity of the full modulation system. Identification of the loss of monotonicity is now undertaken by examining the behavior of the modulation system at the leading and trailing edges.

The full Whitham modulation system exhibits four characteristic speeds $\lambda_1 \leq \lambda_2 \leq \lambda_3 \leq \lambda_4$ that depend on $(k, \overline{\rho}, \overline{u}, a)$. In the case of positive dispersion, the simple wave DSW integral curve is associated with the 2-characteristic (El 2005) and connects the left, right states $(k_1, \rho_1, u_1, 0)$, $(0, \rho_2, u_2, a_2)$, respectively, where $k_1$ is the wavenumber of the wavepacket at the linear wave edge and $a_2$ is the solitary wave amplitude at the soliton edge. Generally, the integral curve can be parametrized by $\overline{\rho} \in [\rho_1, \rho_2]$, $(k(\overline{\rho}), \overline{\rho}, \overline{u}(\overline{\rho}), a(\overline{\rho}))$. The monotonicity condition for a simple wave can therefore be expressed as

$$0 > \frac{d\lambda_2}{d\overline{\rho}} = \frac{\partial \lambda_2}{\partial k} k' + \frac{\partial \lambda_2}{\partial \overline{\rho}} + \frac{\partial \lambda_2}{\partial \overline{u}} \overline{u}' + \frac{\partial \lambda_2}{\partial a} a', \tag{6.8}$$

where primes denote differentiation with respect to $\overline{\rho}$ along the integral curve. At the linear wave edge, the $\lambda_2$ and $\lambda_1$ characteristics merge

$$\nu_1(k, \overline{\rho}, \overline{u}) = \lim_{a \to 0^+} \lambda_1(k, \overline{\rho}, \overline{u}, a) = \lim_{a \to 0^+} \lambda_2(k, \overline{\rho}, \overline{u}, a), \tag{6.9}$$

where $\nu_1$ is the smallest characteristic speed of the modulation system when $a = 0$. This merger of characteristics implies that right differentiability of $\lambda_2$ when $a = 0$ requires

$$\frac{\partial}{\partial a} \lambda_2(k, \overline{\rho}, \overline{u}, 0) = \frac{\partial}{\partial a} \lambda_1(k, \overline{\rho}, \overline{u}, 0) = 0, \tag{6.10}$$

i.e., an $O(a^2)$ dependence of both $\lambda_2$ and $\lambda_1$ on $a$. Using (6.8), (6.9), and (6.10), the breakdown of the monotonicity condition (6.8) can now be identified at the linear wave edge as

$$\lim_{a \to 0^+} \frac{d\lambda_2}{d\overline{\rho}} \bigg|_{k=k_1, \overline{\rho}=\rho_1, \overline{u}=u_1} = \frac{\partial \nu_1}{\partial k} k' + \frac{\partial \nu_1}{\partial \overline{\rho}} + \frac{\partial \nu_1}{\partial \overline{u}} \overline{u}' \bigg|_{k=k_1, \overline{\rho}=\rho_1, \overline{u}=u_1} = 0. \tag{6.11}$$

The zero-amplitude reduction of the modulation system comprises the two dispersionless equations and the conservation of waves (El 2005)

$$\begin{bmatrix} \overline{\rho} \\ \overline{u} \\ k \end{bmatrix}_t + \begin{bmatrix} \overline{u} & \overline{\rho} & 0 \\ c^2/\overline{\rho} & \overline{u} & 0 \\ \omega_{\overline{\rho}} & \omega_{\overline{u}} & \omega_k \end{bmatrix} \begin{bmatrix} \overline{\rho} \\ \overline{u} \\ k \end{bmatrix}_x, \tag{6.12}$$

where $\omega(k, \overline{\rho}, \overline{u})$ is the negative branch of the dispersion relation (2.3). The eigenvalues $v_{1,2,3}$ and associated right eigenvectors $\boldsymbol{r}_{1,2,3}$ for this hyperbolic system are

$$(v_1, \boldsymbol{r}_1) = (\overline{u} - \omega_{0_k}, [0, 0, 1]^{\mathrm{T}}), \tag{6.13a}$$

$$(v_2, \boldsymbol{r}_2) = (\overline{u} - c, [\overline{\rho}(\omega_{0_k} - c), -c(\omega_{0_k} - c), ck - \overline{\rho}\omega_{0_{\overline{\rho}}}]^{\mathrm{T}}), \tag{6.13b}$$

$$(v_3, \boldsymbol{r}_3) = (\overline{u} + c, [\overline{\rho}(\omega_{0_k} + c), c(\omega_{0_k} + c), ck - \overline{\rho}\omega_{0_{\overline{\rho}}}]^{\mathrm{T}}). \tag{6.13c}$$

Note the ordering $v_1 < v_2 < v_3$ due to the $1^+$-DSW admissibility criterion (6.3b). Recalling that the 1-DSW integral curve satisfies (5.4) and (5.5) at the linear wave edge, then (6.11) (breakdown) occurs when

$$\omega_{0_{kk}} \left( \omega_{0_{\overline{\rho}}} + \frac{ck}{\rho} \right) + (c - \omega_{0_k}) \left( \omega_{0_{k\overline{\rho}}} + \frac{c}{\rho} \right) \Bigg|_{k=k_1, \overline{\rho}=\rho_1} = 0. \tag{6.14}$$

A direct computation shows that $\partial v_+ / \partial \rho_1 = 0$ if and only if (6.14) holds, offering a simple test for linear degeneracy once the DSW speed has been computed. The coalescence of two characteristic speeds (nonstrict hyperbolicity) implies linear degeneracy (Dafermos 2009). DSWs described by modulation systems lacking strict hyperbolicity and genuine nonlinearity have been studied for integrable systems (Marchant and Smyth 2006; Pierce and Tian 2006, 2007a,b; Kodama et al. 2008; Grava et al. 2009; Kamchatnov et al. 2012). The results indicate a number of novel features including compound waves (e.g., a DSW attached to a rarefaction), kinks, and enhanced curvature of the DSW oscillation envelope. The latter has led previous authors Kodama et al. (2008) to describe such nonsimple DSWs as having a "wineglass shape" in contrast with simple DSWs that exhibit a "martini glass shape" (see Fig. 1). The linear degeneracy condition (6.14) was given in El et al. (2006) for the nonintegrable Serre equations. Its derivation, however, was wrongly attributed to loss of genuine nonlinearity in the reduced modulation system (6.12) when $a = 0$. Linear degeneracy occurs in this system when

$$\nabla v_i \cdot \boldsymbol{r}_i = 0, \tag{6.15}$$

for some $i \in \{1, 2, 3\}$. $1^+$-DSW admissibility (6.3b) implies that the 2- and 3-characteristic fields do not exhibit linear degeneracy. Evaluation of (6.15) for the 1-characteristic field, however, gives

$$\omega_{kk}(k_1, \rho_1) = 0, \tag{6.16}$$

corresponding to zero dispersion, a different condition than (6.14). In the vicinity of the trailing edge, the $1^+$-DSW self-similar simple wave corresponds to the first characteristic family (6.13a) and satisfies the ODEs

$$\overline{\rho}' = 0, \quad \overline{u}' = 0, \quad k' = -1/\omega_{0_{kk}},$$

where differentiation is with respect to the self-similar variable $x/t$. This demonstrates that the Whitham modulation equations exhibit gradient catastrophe, $|k'| \to \infty$, when the dispersion is zero (6.16). A direct computation demonstrates that $\partial v_+/\partial \rho_2 = 0$ if and only if (6.16) holds. Thus, breaking in the Whitham modulation equations coincides with an extremum of the linear wave edge speed with respect to variation in $\rho_2$.

Breaking in the Whitham equations has been resolved in specific systems by appealing to modulated multiphase waves describing DSW interactions (El 1996; Grava and Tian 2002; Biondini and Kodama 2006; Hoefer and Ablowitz 2007; Ablowitz et al. 2009). A recent study of DSWs in the scalar magma equation shows that the development of zero dispersion for single-step initial data leads to internal multiphase dynamics termed DSW implosion (Lowman and Hoefer 2013). The simple wave assumption no longer holds. This behavior was intuited by Whitham before the development of DSW theory (see Whitham 1974, Sect. 15.4) where breaking of the Whitham modulation equations was hypothesized to "represent a source of oscillations."

An analysis of the soliton wave edge where $k \to 0$ can be similarly undertaken. Recalling that the characteristic speed of the soliton edge is the phase velocity $\overline{u} - \tilde{\omega}_0/\tilde{k}$ (5.11), the breakdown of the monotonicity condition for the positive dispersion case is

$$\lim_{k \to 0^+} \left. \frac{d\lambda_2}{d\overline{\rho}} \right|_{\tilde{k}=\tilde{k}_2, \overline{\rho}=\rho_2, \overline{u}=u_2} = -\frac{\partial}{\partial \tilde{k}}\left(\frac{\tilde{\omega}_0}{\tilde{k}}\right)\tilde{k}' - \frac{\partial}{\partial \overline{\rho}}\left(\frac{\tilde{\omega}_0}{\tilde{k}}\right) + \overline{u}' \bigg|_{\tilde{k}=\tilde{k}_2, \overline{\rho}=\rho_2, \overline{u}=u_2} = 0.$$

Using the 1-DSW locus (5.1) and the characteristic ODE (5.9) leads to the simplification

$$\left(\tilde{k}c - \tilde{\omega}_0\right)\left(\tilde{\omega}_{0_{\overline{\rho}}} + \frac{c\tilde{k}}{\overline{\rho}}\right)\bigg|_{\tilde{k}=\tilde{k}_2, \overline{\rho}=\rho_2} = 0.$$

The positivity of the first factor is equivalent to the admissibility criterion (6.3a), so it is a zero of the second factor,

$$\tilde{\omega}_{0_{\overline{\rho}}} + \frac{c\tilde{k}}{\overline{\rho}}\bigg|_{\tilde{k}=\tilde{k}_2, \overline{\rho}=\rho_2} = 0, \tag{6.17}$$

that offers a new route to linear degeneracy. Recalling that the dispersion relation involves two branches (2.3), care must be taken that the appropriate branch is used in (6.17), which can change when passing through $\tilde{\omega}_0 = 0$. A direct computation verifies that $\partial s_+/\partial \rho_2 = 0$ if and only if (6.17) holds. Therefore, an easy test for linear degeneracy is to find an extremum of $s_+(\rho_1, \rho_2)$ with respect to variations in $\rho_2$. Note that the linear degeneracy condition (6.17) also coincides with a breaking of one of the additional sufficient admissibility conditions in (6.4).

Just as zero dispersion at the linear wave edge can lead to singularity formation in the Whitham equations, the soliton edge can similarly exhibit catastrophe when the phase velocity reaches an extremum

$$\left(\frac{\tilde{\omega}_0}{\tilde{k}}\right)_{\tilde{k}}\Bigg|_{\tilde{k}=\tilde{k}_2,\bar{\rho}=\rho_2} = 0. \tag{6.18}$$

This corresponds to zero conjugate dispersion. When (6.18) is satisfied, wave interactions at the leading edge are expected to occur for larger initial jumps. In contrast to the linear degeneracy criterion, a direct computation verifies that $\partial s_+/\partial\rho_1 = 0$ if and only if (6.18) holds.

The criterion for breakdown of $1^-$-DSWs is the same as (6.14), (6.16) with $1 \to 2$ and (6.17), (6.18) with $2 \to 1$. In summary, two mechanisms at each DSW edge for the breakdown of the simple wave assumption have been identified: the loss of monotonicity (linear degeneracy) (6.14), (6.17) or gradient catastrophe in the Whitham modulation equations due to zero dispersion (6.16), (6.18). These behaviors can be succinctly identified via extrema in the DSW speeds as

$$1^+-\text{DSW}: \quad \begin{aligned} &\text{linear degeneracy} &&\frac{\partial v_+}{\partial\rho_1} = 0 \ \text{ or } \ \frac{\partial s_+}{\partial\rho_2} = 0, \\ &\text{gradient catastrophe} &&\frac{\partial v_+}{\partial\rho_2} = 0 \ \text{ or } \ \frac{\partial s_+}{\partial\rho_1} = 0, \end{aligned} \tag{6.19a}$$

$$1^--\text{DSW}: \quad \begin{aligned} &\text{linear degeneracy} &&\frac{\partial v_-}{\partial\rho_2} = 0 \ \text{ or } \ \frac{\partial s_-}{\partial\rho_1} = 0, \\ &\text{gradient catastrophe} &&\frac{\partial v_-}{\partial\rho_1} = 0 \ \text{ or } \ \frac{\partial s_-}{\partial\rho_2} = 0. \end{aligned} \tag{6.19b}$$

The negation of these breakdown criteria are further necessary admissibility criteria, additional to (6.1a)–(6.1c), for the validity of the simple wave DSW construction.

## 7 Weak DSWs

The jump conditions for an admissible 1-DSW presented in Sect. 5 apply generally to dispersive Eulerian fluids satisfying hypotheses A1–A5. They can be determined explicitly in the case of weak DSWs. An asymptotic analysis of the jump conditions is presented below assuming a weak 1-DSW corresponding to a small jump in density

$$\rho_2 = \rho_1 + \Delta, \qquad |\Delta| \ll 1.$$

Two approaches are taken. First, asymptotics of the Whitham–El simple wave DSW closure theory are applied, and second, direct KdV asymptotics of the dispersive Euler equations are used.

### 7.1 Linear Wave Edge

Expanding the linear wave edge speed (5.7) yields

$$v_j(\rho_1, \rho_1 + \Delta) \sim \lim_{\rho_2 \to \rho_1} v_j(\rho_1, \rho_2) + \frac{\partial}{\partial \rho_2} v_j(\rho_1, \rho_2) \Delta. \tag{7.1}$$

Using the long-wave asymptotics of the dispersion relation (2.4) and the initial condition for the integral curve (5.6), the first term is

$$\lim_{\rho_2 \to \rho_1} v_j(\rho_1, \rho_2) = u_1 - \lim_{k \to 0} \omega_{0k} = u_1 - c_1.$$

The derivative term in (7.1) for the case $j = 1$ is evaluated using (5.5)–(5.7)

$$\lim_{\rho_2 \to \rho_1} \frac{\partial}{\partial \rho_2} v_1(\rho_1, \rho_2) = \lim_{\rho_2 \to \rho_1} -\omega_{0kk} \frac{\partial k}{\partial \rho_2} = \lim_{\rho_2 \to \rho_1} \omega_{0kk} \frac{dk}{d\rho_1}$$

$$= \lim_{k \to 0} \omega_{0kk} \frac{c_1 k / \rho_1 + \omega_{0\overline{\rho}}}{c_1 - \omega_{0k}}$$

$$= -2 \left( \frac{c_1}{\rho_1} + c_1' \right). \tag{7.2}$$

The second equality in (7.2) involves differentiation with respect to the initial "time" $\rho_2$, which, due to uniqueness of solutions to the initial value problem, satisfies

$$\frac{\partial k}{\partial \rho_2}(\rho_1; \rho_2) = -\frac{dk}{d\rho_1}(\rho_1; \rho_2). \tag{7.3}$$

The last equality in (7.2) follows from the weak dispersion asymptotics (2.4). A similar computation for the $j = 2$ case gives

$$\lim_{\rho_2 \to \rho_1} \frac{\partial}{\partial \rho_2} v_2(\rho_1, \rho_2) = \lim_{\rho_2 \to \rho_1} \overline{u}'(\rho_2) - \omega_{0k\overline{\rho}} - \omega_{0kk} \frac{dk}{d\overline{\rho}}$$

$$= -\frac{c_1}{\rho_1} - \left( \lim_{k \to 0} \omega_{0k\overline{\rho}} + \omega_{0kk} \frac{c_1 k / \rho_1 + \omega_{0\overline{\rho}}}{c_1 - \omega_{0k}} \right)$$

$$= \frac{c_1}{\rho_1} + c_1'.$$

Combining this result with the other speed calculation gives

$$v_j(\rho_1, \rho_1 + \Delta) \sim u_1 - c_1 + (-1)^j (3 - j) \left( \frac{c_1}{\rho_1} + c_1' \right) \Delta, \qquad |\Delta| \ll 1. \tag{7.4}$$

The corresponding wavenumber at the linear wave edge can also be determined perturbatively. Note that a Taylor expansion of $k_1 = k(\rho_1; \rho_1 + \Delta)$ for small $\Delta$ is not valid because $k(\rho; \rho_1)$ is not analytic in a neighborhood of $\rho_1$, exhibiting a square root branch point. However, $k_1^2$ is analytic, so that upon Taylor expansion, the use of (7.3) and (2.4) yields

$$k_j \sim \frac{2}{3|\mu|} \left( \frac{c_1}{\rho_1} + c_1' \right) \sqrt{|\Delta|}, \qquad j = 1, 2, \qquad |\Delta| \ll 1,$$

the wavenumber of the linear wavepacket at a weak $1^{\pm}$-DSW's linear wave edge. Note that the wavenumber is independent of the sign of dispersion.

### 7.2 Soliton Edge

The soliton edge speed is expanded for a small density jump as

$$s_j(\rho_1, \rho_1 + \Delta) = \lim_{\rho_2 \to \rho_1} s_j(\rho_1, \rho_2) + \frac{\partial}{\partial \rho_2} s_j(\rho_1, \rho_2)\Delta + \cdots.$$

Using the expansion (2.4), the definition (5.8), the expression (5.11), and the initial condition (5.10) gives

$$\lim_{\rho_2 \to \rho_1} s_j(\rho_1, \rho_2) = u_1 - \lim_{\tilde{k} \to 0} \frac{\tilde{\omega}_0(\tilde{k}, \rho_1)}{\tilde{k}} = u_1 - c_1.$$

To compute the limit $\frac{\partial}{\partial \rho_2} s_j(\rho_1, \rho_1)$ necessitates different considerations for each $j$. When $j = 1$, (5.11) gives

$$\lim_{\rho_2 \to \rho_1} \frac{\partial}{\partial \rho_2} s_1(\rho_1, \rho_2) = \lim_{\rho_2 \to \rho_1} -\frac{\tilde{\omega}_{0_{\tilde{k}}}\tilde{k} - \tilde{\omega}_0}{\tilde{k}^2} \frac{\partial \tilde{k}}{\partial \rho_2}$$

$$= \lim_{\rho_2 \to \rho_1} \frac{\tilde{\omega}_{0_{\tilde{k}}}\tilde{k} - \tilde{\omega}_0}{\tilde{k}^2} \frac{d\tilde{k}}{d\rho_1}$$

$$= \lim_{\tilde{k} \to 0} \frac{(\tilde{\omega}_{0_{\tilde{k}}}\tilde{k} - \tilde{\omega}_0)(c_1\tilde{k}/\rho_1 + \tilde{\omega}_{0_{\bar{\rho}}})}{\tilde{k}^2(c_1 - \tilde{\omega}_{0_{\tilde{k}}})}$$

$$= -\frac{2}{3}\left(\frac{c_1}{\rho_1} + c_1'\right).$$

When $j = 2$, the limit is similarly computed as

$$\lim_{\rho_2 \to \rho_1} \frac{\partial}{\partial \rho_2} s_2(\rho_1, \rho_2) = \lim_{\rho_2 \to \rho_1} u'(\rho_1) - \frac{\tilde{\omega}_{0_{\bar{\rho}}}}{\tilde{k}} - \frac{\tilde{\omega}_{0_{\tilde{k}}}\tilde{k} - \tilde{\omega}_0}{\tilde{k}^2} \frac{d\tilde{k}}{d\bar{\rho}}$$

$$= \lim_{\tilde{k} \to 0} -\frac{c_1}{\rho_1} - \frac{\tilde{\omega}_{0_{\bar{\rho}}}}{\tilde{k}} - \frac{(\tilde{\omega}_{0_{\tilde{k}}}\tilde{k} - \tilde{\omega}_0)(c_1\tilde{k}/\rho_1 + \tilde{\omega}_{0_{\bar{\rho}}})}{\tilde{k}^2(c_1 - \tilde{\omega}_{0_{\tilde{k}}})}$$

$$= -\frac{1}{3}\left(\frac{c_1}{\rho_1} + c_1'\right).$$

Combining these results gives the asymptotic soliton edge speed

$$s_j(\rho_1, \rho_1 + \Delta) \sim u_1 - c_1 - \frac{3-j}{3}\left(\frac{c_1}{\rho_1} + c_1'\right)\Delta, \qquad |\Delta| \ll 1. \qquad (7.5)$$

### 7.3 Admissibility: Positive and Negative Dispersion

By insertion of the DSW speeds (7.4) and (7.5) into the general admissibility criteria, it is found that the $1^+$-DSW criteria (6.1a)–(6.1c) are satisfied if and only if $\Delta > 0$ and sgn $\omega_{kk} > 0$. Similarly, the $1^-$-DSW criteria (6.2a)–(6.2c) hold if and only if $\Delta > 0$ and sgn $\omega_{kk} < 0$. Hence, the notation $1^{\pm}$-DSW associated with the dispersion sign is justified for weak DSWs.

In the notation of (6.6), the weak $1^{\pm}$-DSW speeds are

$$s_{\pm}^{(1)}(\rho_1, \rho_1 + \Delta) \sim u_1 - c_1 - \frac{3 \mp 1}{6}\left(\frac{c_1}{\rho_1} + c_1'\right)\Delta, \tag{7.6a}$$

$$v_{\pm}^{(1)}(\rho_1, \rho_1 + \Delta) \sim u_1 - c_1 - \frac{1 \pm 3}{2}\left(\frac{c_1}{\rho_1} + c_1'\right)\Delta, \qquad 0 < \Delta \ll 1, \tag{7.6b}$$

where the superscript denotes the association with a 1-DSW. Notably, the DSW speeds (7.6a) and (7.6b) differ from the dissipatively regularized shock speed (4.14) only in the numerical coefficient of the $(c_1/\rho_1 + c_1')\Delta$ term. A similar analysis shows that the 2-DSW locus (5.2) requires a *negative* jump in density and yields the speeds

$$s_{\pm}^{(2)}(\rho_2 + \Delta, \rho_2) \sim u_2 + c_2 + \frac{3 \mp 1}{6}\left(\frac{c_2}{\rho_2} + c_2'\right)\Delta,$$

$$v_{\pm}^{(2)}(\rho_2 + \Delta, \rho_2) \sim u_2 + c_2 + \frac{1 \pm 3}{2}\left(\frac{c_2}{\rho_2} + c_2'\right)\Delta, \qquad 0 < \Delta \ll 1.$$

### 7.4 Stationary Soliton Edge

Choosing the reference frame moving with the $1^{\pm}$-DSW soliton edge so that $s_{\pm}^{(1)} = 0$ results in the relations

$$\Delta_{\pm} \sim \frac{2\rho_1 c_1}{(1 \mp 1/3)(c_1 + \rho_1 c_1')}(M_1 - 1),$$

$$M_{2,\pm} \sim 1 - 2^{\pm 1}(M_1 - 1), \qquad 0 < M_1 - 1 \ll 1,$$

which differ from their classical counterparts (4.15) only by a numerical coefficient. Upstream supersonic flow through a weak, admissible DSW results in downstream subsonic flow as in the classical case.

### 7.5 KdV DSWs

An alternative method to derive weak DSW properties is to consider the weakly non-linear behavior of the dispersive Euler equations directly. Inserting the multiple scales expansion

$$\rho = \rho_1 + \Delta \rho^{(1)}(\xi, T) + \Delta^2 \rho^{(2)}(\xi, T) + \cdots,$$
$$u = u_1 - \Delta u^{(1)}(\xi, T) + \Delta^2 u^{(2)}(\xi, T) + \cdots,$$
$$\xi = \Delta^{1/2}[x - (u_1 - c_1)t], \qquad T = \Delta^{3/2}t, \qquad 0 < \Delta \ll 1,$$

into (2.1), equating like powers of $\Delta$ to $\mathcal{O}(\Delta^{5/2})$, and recalling the assumed small wavenumber behavior of the dispersion relation (2.4) yields the KdV equation

$$u_T^{(1)} - \left(1 + \frac{\rho_1 c_1'}{c_1}\right) u^{(1)} u_\xi^{(1)} + \mu u_{\xi\xi\xi}^{(1)} = 0, \qquad \rho^{(1)} = \frac{\rho_1}{c_1} u^{(1)}. \qquad (7.7)$$

The initial data (2.5) along the 1-DSW locus (5.1) leads to the identification

$$u^{(1)}(\xi, 0) = \begin{cases} 0 & \xi < 0 \\ c_1/\rho_1 & \xi > 0. \end{cases} \qquad (7.8)$$

The large-$T$ behavior of $u^{(1)}$ satisfying (7.7) for the initial data (7.8) results in a DSW whose structure and edge speeds depend on sgn $\mu$. For negative dispersion, $\mu < 0$, the DSW is oriented such that the leading, leftmost edge is characterized by a positive, bright soliton. The positive dispersion case is equivalent to the negative dispersion case by the transformations $x \to -x$, $t \to -t$, and $u^{(1)} \to -u^{(1)}$. Therefore, the leading, leftmost edge is the linear wave edge and the trailing edge is characterized by a negative, dark soliton. Scaling the KdV DSW speeds back to the $(x, t)$ variables results precisely in the admissible, approximate weak $1^{\pm}$-DSW speeds (7.6a) and (7.6b). The KdV DSW provides additional information, the approximate amplitude of the soliton edge

$$1^+ - \text{DSW}: \quad \rho(s_+ t, t) \sim \rho_1 \left(1 - \frac{\rho_1}{c_1^2} \Delta\right),$$

$$1^- - \text{DSW}: \quad \rho(s_- t, t) \sim \rho_1 \left(1 + 2\frac{\rho_1}{c_1^2} \Delta\right).$$

## 7.6 Discussion

The analysis of this section has yielded the behavior of weak Eulerian DSWs in the context of assumptions A1–A5 and the admissibility criteria (6.1a)–(6.2c). For classical, weak 1-shocks (2-shocks), the dispersionless Riemann invariant $r_2$ ($r_1$) is constant across the shock to third order in the jump height $\Delta$ (Whitham 1974). Recalling that the DSW loci (5.1), (5.2) correspond to constancy of a Riemann invariant (simple wave condition), the classical Hugoniot loci and the DSW loci for weak shocks are the same to $\mathcal{O}(\Delta^3)$. However, the shock speeds differ at $\mathcal{O}(\Delta)$. The universal properties of weak shocks regularized by positive/negative dispersion and dissipation are depicted in Fig. 3. The jump height $\Delta$, upstream density $\rho_1$, and pressure law $P(\rho)$ impart
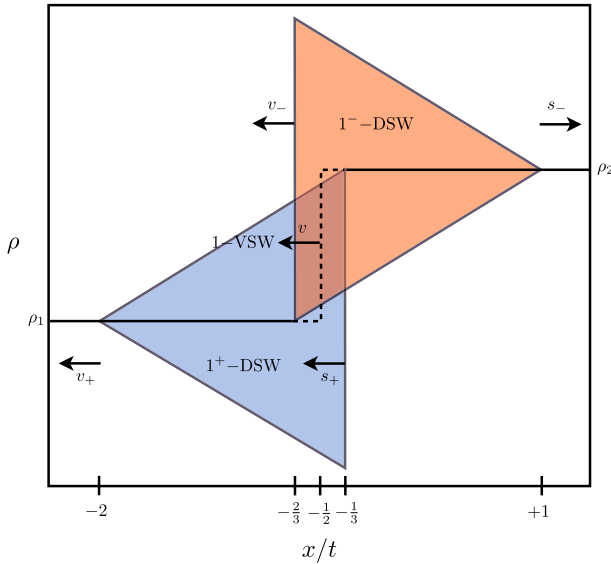
**Fig. 3** Universal properties of weak $1^{\pm}$-DSWs with a weak 1-viscous shock wave (VSW). DSWs are represented by their envelopes and edge speeds. Speeds are in units of $(c_1/\rho_1 + c_1')\Delta$ and $u_1 = c_1$ for simplicity

only a uniform scaling of the shock speeds by $(c_1/\rho_1 + c_1')\Delta$ and a relative scaling of the $1^{\pm}$-DSW soliton amplitudes by $\rho_1\Delta/c_1^2$. All shock speeds differ, showcasing the distinguishing properties of each regularization type. $1^-$-DSWs exhibit backpropagation, whereas $1^+$-DSWs and 1-VSWs (viscous shocks) do not. The prominent soliton edge of a $1^-$-DSW ($1^+$-DSW) propagates faster (slower) than a classical shock. By continuity and the discussion of admissibility, it is expected that moderate amplitude DSWs for Eulerian fluids with a fixed sign of the dispersion exhibit a structure similar to that pictured in Fig. 1. This is indeed the case for the example fluids considered in this work; see Sect. 9.

## 8 Dispersive Breaking Time

In the small dispersion regime, the hydrodynamic dispersionless system (4.4) asymptotically describes the evolution of smooth initial data until breaking occurs. One can therefore use the breaking time estimates from Sect. 4.1 to estimate the time at which dispersive terms become important. This result was applied to the NLS equation with $c(\rho) = \rho^{1/2}$ in Forest and McLaughlin (1998) to estimate the onset of oscillations in fiber-optic pulse propagation. Here, the breaking time estimates are applied to polytropic gases with sound speeds $c(\rho) = p^{1/2}\rho^{p/2}$, $0 < p < 2$ (e.g., gNLS with power-law nonlinearity and gSerre). Generalizations using Lax's theory developed in Sect. 4.1 are straightforward.
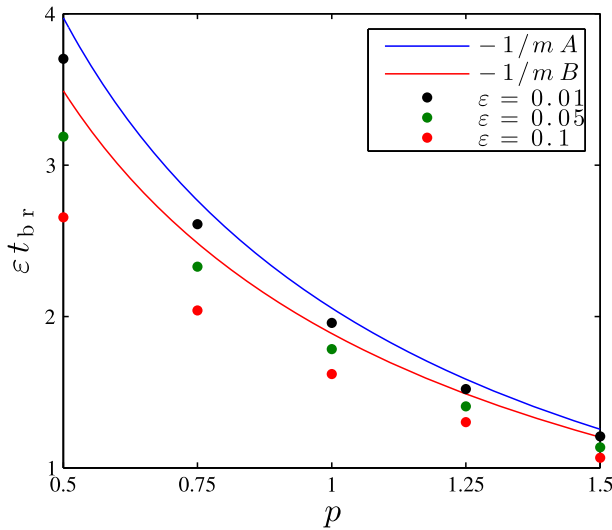
**Fig. 4** Breaking time bounds (*solid lines*) and numerically computed breaking times (*filled circles*) for gNLS with power-law nonlinearity $f(\rho) = \rho^p$ and slowly varying Gaussian initial data (8.1)

The flow considered is a slowly varying Gaussian on a quiescent background

$$u(x, 0) = 0, \qquad \rho(x, 0) = 1 + \exp[-(\varepsilon x)^2], \qquad 0 < \varepsilon \ll 1. \tag{8.1}$$

Slowly varying initial data ensure the applicability of the dispersionless system (4.4) up to breaking when $t = \mathcal{O}(1/\varepsilon)$. This choice of initial data has been used in photonic DSW experiments (Barsi et al. 2012).

Figure 4 shows the results for the gNLS equation (3.1) with power-law nonlinearity $f(\rho) = \rho^p$. The solid curves (——) correspond to the upper and lower bounds on the dispersionless breaking time estimates (4.11), and bullets (●) correspond to numerically computed breaking times for several choices of $p$ and $\varepsilon$. The breaking time from simulations is defined to be the time at which the density first develops one full oscillation in the breaking region. For $|\varepsilon| \ll 1$, the bounds (4.11) accurately estimate the breaking time across a range of nonlinearities $p$. Note that, for these dispersive Euler models and class of initial data, $\varepsilon \lessgtr 0.01$ is required to obtain agreement with the dispersionless estimates.

## 9 Large Amplitude gNLS DSWs

The general Whitham–El simple wave DSW theory is now implemented for the gNLS equation.

To simplify the presentation, and without loss of generality, the independent and dependent variables in (2.2) will be scaled so that the initial jump in density (2.5) is positive, from unit density

$$\rho_1 = 1, \qquad \rho_2 = \Delta > 1,$$

so that 1-DSWs will be considered. Then, according to the 1-DSW locus (5.1) of admissible states, the jump in velocity satisfies

$$u_2 = u_1 - \int_1^\Delta \left( \frac{f'(\rho)}{\rho} \right)^{1/2} d\rho.$$

## 9.1 General Properties

The gNLS equation exhibits positive dispersion so that DSWs are of the $1^+$ variety. Substituting the expressions (3.8) and (5.4) into the ODEs (5.3) and (5.9) results in the initial value problems

$$\frac{dk}{d\overline{\rho}} = -k \frac{\frac{1}{\overline{\rho}} \left[ 1 + \frac{k^2}{4\overline{\rho} f'(\overline{\rho})} \right]^{1/2} + \frac{1}{2\overline{\rho}} + \frac{f''(\overline{\rho})}{2 f'(\overline{\rho})}}{1 + \frac{k^2}{2\overline{\rho} f'(\overline{\rho})} - \left[ 1 + \frac{k^2}{4\overline{\rho} f'(\overline{\rho})} \right]^{1/2}}, \qquad k(\Delta) = 0 \qquad (9.1)$$

for the determination of the linear wave edge speed, and

$$\frac{d\tilde{k}}{d\overline{\rho}} = -\tilde{k} \frac{\frac{1}{\overline{\rho}} \left[ 1 - \frac{\tilde{k}^2}{4\overline{\rho} f'(\overline{\rho})} \right]^{1/2} + \frac{1}{2\overline{\rho}} + \frac{f''(\overline{\rho})}{2 f'(\overline{\rho})}}{1 - \frac{\tilde{k}^2}{2\overline{\rho} f'(\overline{\rho})} - \left[ 1 - \frac{\tilde{k}^2}{4\overline{\rho} f'(\overline{\rho})} \right]^{1/2}}, \qquad \tilde{k}(1) = 0 \qquad (9.2)$$

for the soliton edge speed. In (9.2), it is possible for the quantity within the square roots to pass through zero. When this occurs, an appropriate branch of the dispersion relation should be used so that the conjugate wavenumber remains real valued.

Recalling Remark 1 in Sect. 5.2, the transformation

$$\alpha(\overline{\rho}) = \frac{\omega_0(k, \overline{\rho})}{c(\overline{\rho})k} = \left[ 1 + \frac{k^2}{4\overline{\rho} f'(\overline{\rho})} \right]^{1/2}$$

simplifies (9.1) to the ODE

$$\frac{d\alpha}{d\overline{\rho}} = -\frac{1}{2}(1 + \alpha) \left[ \frac{1}{\overline{\rho}} + \frac{(2\alpha - 1) f''(\overline{\rho})}{(2\alpha + 1) f'(\overline{\rho})} \right], \qquad (9.3)$$

with initial condition

$$\alpha(\Delta) = 1. \qquad (9.4)$$

The analogous transformation for the conjugate variables

$$\tilde{\alpha}(\overline{\rho}) = \frac{\tilde{\omega}_0(\tilde{k}, \overline{\rho})}{c(\overline{\rho})\tilde{k}} = \left[1 - \frac{\tilde{k}^2}{4c(\overline{\rho})^2}\right]^{1/2} \tag{9.5}$$

transforms (9.2) to the same equation (9.3) with $\alpha \to \tilde{\alpha}$ and the initial condition

$$\tilde{\alpha}(1) = 1. \tag{9.6}$$

Upon solving the initial value problems for $\alpha$ and $\tilde{\alpha}$, the linear wave and soliton edge speeds are found from (5.7) and (5.11), respectively, which take the form

$$v_+ = u_1 + \frac{1 - 2\alpha(1)^2}{\alpha(1)}\sqrt{f'(1)}, \tag{9.7a}$$

$$s_+ = u_1 - \tilde{\alpha}(\Delta)\sqrt{\Delta f'(\Delta)} - \int_1^\Delta \left[\frac{f'(\rho)}{\rho}\right]^{1/2} d\rho, \tag{9.7b}$$

in the $\alpha$, $\tilde{\alpha}$ variables. The weak DSW results (7.4) and (7.5) give the approximations

$$v_+ \sim u_1 - \sqrt{f'(1)}\left\{1 + \left[3 + \frac{f''(1)}{f'(1)}\right](\Delta - 1)\right\}, \tag{9.8a}$$

$$s_+ \sim u_1 - \sqrt{f'(1)}\left\{1 + \frac{1}{6}\left[3 + \frac{f''(1)}{f'(1)}\right](\Delta - 1)\right\}, \quad 0 < \Delta - 1 \ll 1. \tag{9.8b}$$

Equating the soliton speed in (9.7b) to the soliton/amplitude speed relation in (3.10) gives an implicit relation for the dark soliton minimum $\rho_{\min}$ in terms of the background density $\Delta$

$$\tilde{\alpha}(\Delta)^2 \Delta f'(\Delta) = \frac{2\rho_{\min}}{\Delta - \rho_{\min}}\left|f(\Delta) - \frac{1}{\Delta - \rho_{\min}}\int_{\rho_{\min}}^\Delta f(\rho)d\rho\right|. \tag{9.9}$$

A direct computation shows that neither linear degeneracy (6.14) nor a sign of dispersion change (6.16) occurs at the linear wave edge. However, at the soliton edge, there are several distinguished values of $\tilde{\alpha}(\Delta)$ with physical ramifications. The modulation theory breaks down due to singular derivative formation in (9.3) when

$$\tilde{\alpha}(\Delta = \Delta_s) = -\frac{1}{2}.$$

From the denominator in (5.9), singularity formation occurs precisely when $\tilde{\omega}_{0\tilde{k}} = c(\Delta)$. A direct computation shows that $\tilde{\omega}_0$ is a concave function of $\tilde{k}$, which implies

$\tilde{\omega}_0/\tilde{k} > \tilde{\omega}_{0_{\tilde{k}}} = c(\Delta)$ so that singularity formation coincides with the violation of the admissibility criterion (6.3a).

From the initial condition (9.6) and the ODE (9.3), $\tilde{\alpha}(\Delta)$ decreases from 1 for increasing $\Delta$ sufficiently close to 1. The value of $\tilde{\alpha}$ at which its derivative is zero, from (9.3), is

$$\tilde{\alpha}_{\min}(\Delta) = \frac{\Delta f''(\Delta) - f'(\Delta)}{2[\Delta f''(\Delta) + f'(\Delta)]}.$$

So long as

$$\tilde{\alpha}(\Delta) > \max\left[\tilde{\alpha}_{\min}(\Delta), -\frac{1}{2}\right],$$

the right-hand side of (9.3) is strictly negative and finite. Since $\alpha$ satisfies the same ODE as $\tilde{\alpha}$, if $\tilde{\alpha}_{\min} < 1$, $\alpha(1)$ is an *increasing* function for all $\Delta$ and $\tilde{\alpha}(\Delta)$ is a *decreasing* function of $\Delta$ until $\tilde{\alpha}(\Delta) = \max(\tilde{\alpha}_{\min}(\Delta), -1/2)$.

As $\Delta$ is increased from 1, cavitation (a point of zero density or *vacuum point*) first occurs when $\rho_{\min} = 0$, corresponding to a black soliton at the trailing edge, moving with the background flow speed $\bar{u}(\Delta)$. Since necessarily $\Delta > \rho_{\min}$, (9.9) implies that a vacuum point first occurs when

$$\tilde{\alpha}(\Delta = \Delta_v) = 0. \tag{9.10}$$

For larger jumps $\Delta > \Delta_v$, the vacuum point is expected to develop in the interior of the DSW (El et al. 1995, 2007). According to the transformation (9.5), when $\tilde{\alpha}$ crosses zero, the branch of the conjugate dispersion changes sign.

Using Galilean invariance, it is convenient to consider the reference frame moving with the soliton edge so that $s_+ = 0$. In such a frame, given the upstream supersonic flow velocity $u_1 > 1$, the density jump $\Delta$ is determined from (9.7b) and the downstream flow velocity satisfies $u_2 = \tilde{\alpha}(\Delta)\sqrt{\Delta f'(\Delta)}$. Then, for $\Delta < \Delta_v$, $\tilde{\alpha}(\Delta) > 0$ so that $u_2 > 0$. But, when $\Delta > \Delta_v$, cavitation occurs and $\tilde{\alpha}(\Delta)$ changes sign causing $u_2 < 0$. Counterintuitively, the dispersive fluid flows *into* the DSW from both sides upon the generation of a vacuum point. This behavior has been observed in NLS (Gurevich and Krylov 1987) and photorefractive gNLS (El et al. 2007).

At the soliton edge, linear degeneracy (6.17) occurs when

$$\tilde{\omega}_{0_{\bar{\rho}}} + \frac{c\tilde{k}}{\bar{\rho}} = c\tilde{k}\left[\frac{f'(\Delta) + \Delta f''(\Delta)}{2\Delta f'(\Delta)\tilde{\alpha}} + \frac{1}{\Delta}\right] = 0. \tag{9.11}$$

The only way for this to occur is for $\tilde{\omega}_0$ to change to another branch of the conjugate dispersion relation, i.e., for $\tilde{\alpha}$ to pass through 0. Then, from (9.11), the value of $\tilde{\alpha}$ at which linear degeneracy occurs is

$$\tilde{\alpha}_l(\Delta) = -\frac{1}{2}\left[1 + \frac{\Delta f''(\Delta)}{f'(\Delta)}\right]. \tag{9.12}$$

According to the assumptions on $f$ (3.7), $\tilde{\alpha}_l < 0$ as required. Since the linear degeneracy condition (9.11) amounts to $ds_+/d\Delta = 0$ [recall (6.19a)], the distinguished value $\tilde{\alpha}_l$ coincides with an extremum of the soliton edge speed as the jump height $\Delta$ is varied.

A direct computation verifies that the zero dispersion criterion (6.18) does not occur. The admissibility criteria (6.1a) and (6.1b) correspond to $\tilde{\alpha}(\Delta) < 1$ and $\alpha(1) < 1$, which are true generically. In summary, so long as $\tilde{\alpha}_{\min} < -1/2$, $\tilde{\alpha}(\Delta)$ is a decreasing function that can attain the distinguished values $\tilde{\alpha} = 0$ when $\Delta = \Delta_v$ corresponding to a vacuum point or cavitation, $\tilde{\alpha} = \tilde{\alpha}_l$ when $\Delta = \Delta_l$ coinciding with linear degeneracy and the breakdown of the simple wave criterion, and $\tilde{\alpha} = -1/2$ when $\Delta = \Delta_s$ leading to singularity formation. For $\Delta < \Delta_l$, the only admissibility criterion left to verify is the leading and trailing edge ordering (6.1c).

The DSW regularization is completed upon solving the ODE (9.3). This equation is separable for nonlinearity satisfying $f'(\rho) \pm \rho f''(\rho) = 0$. Recalling the admissible nonlinearity (3.7), the cases of interest are $f(\rho) = \kappa \rho^p$, $p > 0$, corresponding to polytropic superfluids. This class of nonlinearity is now considered.

9.2 Power-Law Nonlinearity

With the choice (3.2) of power-law nonlinearity, the speed of sound is $c(\rho) = p^{1/2} \rho^{p/2}$. Equation (9.3) becomes the separable equation

$$\frac{-2(1 + 2\alpha)}{(1 + \alpha)(2 - p + 2p\alpha)} d\alpha = \frac{d\overline{\rho}}{\overline{\rho}}. \tag{9.13}$$

Using the initial condition (9.4), (9.13) is integrated to

$$\frac{1 + \alpha(1)}{2} \left[ \frac{2 - p + 2p\alpha(1)}{2 + p} \right]^{2(p-1)/p} = \Delta^{(3p-2)/2}, \qquad p \neq \frac{2}{3}, \tag{9.14a}$$

$$2 \ln \left[ \frac{1 + \alpha(1)}{2} \right] + \frac{1}{1 + \alpha(1)} - \frac{1}{2} = \frac{2}{3} \ln \Delta, \qquad p = \frac{2}{3}, \tag{9.14b}$$

and for (9.6), (9.13) is integrated to

$$\frac{1 + \tilde{\alpha}(\Delta)}{2} \left[ \frac{2 - p + 2p\tilde{\alpha}(\Delta)}{2 + p} \right]^{2(p-1)/p} = \Delta^{(2-3p)/2}, \qquad p \neq \frac{2}{3}, \tag{9.15a}$$

$$2 \ln \left[ \frac{1 + \tilde{\alpha}(\Delta)}{2} \right] + \frac{1}{1 + \tilde{\alpha}(\Delta)} - \frac{1}{2} = -\frac{2}{3} \ln \Delta, \qquad p = \frac{2}{3}, \tag{9.15b}$$

the integrals existing so long as

$$\alpha(1), \; \tilde{\alpha}(\Delta) > \frac{p-2}{2p} = \tilde{\alpha}_{\min}.$$

The linear wave and soliton edge speeds are then determined via (9.7a) and (9.7b)

$$\frac{v_+ - u_1}{c_1} = \frac{1 - 2\alpha(1)^2}{\alpha(1)}, \tag{9.16a}$$

$$\frac{s_+ - u_1}{c_1} = -\Delta^{p/2} \left[ \frac{2}{p} + \tilde{\alpha}(\Delta) \right] + \frac{2}{p}. \tag{9.16b}$$

Equations (9.14a) and (9.15a) can be solved explicitly for $\alpha$ in several cases

$$p = \frac{1}{2} : \quad \begin{cases} \alpha(1) = \frac{25}{16}\Delta^{1/4} - \frac{3}{2} + \frac{5}{16}\left(25\Delta^{1/2} - 16\Delta^{1/4}\right)^{1/2}, \\ \tilde{\alpha}(\Delta) = \frac{25}{16}\Delta^{-1/4} - \frac{3}{2} + \frac{5}{16}\left(25\Delta^{-1/2} - 16\Delta^{-1/4}\right)^{1/2}, \end{cases} \tag{9.17a}$$

$$p = 1 : \quad \begin{cases} \alpha(1) = 2\Delta^{1/2} - 1, \\ \tilde{\alpha}(\Delta) = 2\Delta^{-1/2} - 1, \end{cases} \tag{9.17b}$$

$$p = 2 : \quad \begin{cases} \alpha(1) = \frac{1}{2}\left(\sqrt{1 + 8\Delta^2} - 1\right), \\ \tilde{\alpha}(\Delta) = \frac{1}{2}\left(\sqrt{1 + 8\Delta^{-2}} - 1\right), \end{cases} \tag{9.17c}$$

providing explicit expressions for the 1-DSW linear wave and soliton edge speeds

$$p = \frac{1}{2} : \quad \begin{cases} \frac{v_+ - u_1}{c_1} = \frac{16 - \frac{1}{8}\left[25\Delta^{1/4} - 24 + 5\sqrt{25\Delta^{1/2} - 16\Delta^{1/4}}\right]^2}{25\Delta^{1/4} - 24 + 5\sqrt{25\Delta^{1/2} - 16\Delta^{1/4}}}, \\ \frac{s_+ - u_1}{c_1} = -\frac{5}{2}\Delta^{1/4} + \frac{39}{16} - \frac{5}{16}\sqrt{25 - 16\Delta^{1/4}}, \end{cases} \tag{9.18a}$$

$$p = 1 : \quad \begin{cases} \frac{v_+ - u_1}{c_1} = -\frac{8\Delta - 8\Delta^{1/2} + 1}{2\Delta^{1/2} - 1}, \\ \frac{s_+ - u_1}{c_1} = -\Delta^{1/2}, \end{cases} \tag{9.18b}$$

$$p = 2 : \quad \begin{cases} \frac{v_+ - u_1}{c_1} = -2\frac{4\Delta^2 - \sqrt{1 + 8\Delta^2}}{\sqrt{1 + 8\Delta^2} - 1}, \\ \frac{s_+ - u_1}{c_1} = -\frac{1}{2}\left(\Delta - 2 + \sqrt{8 + \Delta^2}\right). \end{cases} \tag{9.18c}$$

The cubic NLS case (9.18b) agrees with the original result in Gurevich and Krylov (1987).

The distinguished values of the jump height $\Delta$ predict different DSW behavior as $p$ varies. The large-$\Delta$ behavior of (9.15a) and the fact that $\tilde{\alpha}(\Delta)$ is a decreasing function of $\Delta$ prove that

$$\tilde{\alpha}(\Delta) \searrow \frac{p-2}{2p} > -\frac{1}{2}, \qquad \Delta \to \infty, \qquad p > 1, \tag{9.19}$$

precluding the possibility of singularity formation when $p > 1$. Furthermore, when $p \geq 2$, (9.19) prohibits cavitation in the DSW because $\tilde{\alpha}(\Delta) > 0$.

The cavitation condition (9.10) can be used along with (9.15a) to determine $\Delta_v(p)$, the value of $\Delta$ at which a vacuum point is predicted to appear

$$\Delta_v(p) = 2^{2/(3p-2)} \left( \frac{2-p}{2+p} \right)^{4(1-p)/[p(3p-2)]}, \qquad 0 < p < 2, \qquad p \neq \frac{2}{3}, \tag{9.20a}$$

$$\lim_{p \to 2/3} \Delta_v(p) = \frac{8}{\exp(3/4)} \approx 3.78. \tag{9.20b}$$

For $p$ approaching 2, the vacuum jump $\Delta_v$ increases without bound. The limiting behavior for $p \to 0$ is $\Delta_v(p) \to e^2/2 \approx 3.69$.

The DSW soliton speed exhibits a minimum (maximum in absolute value) for $0 < p < 1$ corresponding to the onset of linear degeneracy in the modulation system. The value of the jump height $\Delta_l$ at the linear degeneracy point is found by inserting (9.12) into (9.15a) and solving for $\Delta$

$$\Delta_l(p) = \left[ \frac{1}{4}(2-p)(1-p)^{2-2/p} \right]^{2/(2-3p)}, \qquad 0 < p < 1, \qquad p \neq \frac{2}{3}, \tag{9.21a}$$

$$\Delta_l(2/3) = \frac{27}{\exp(3/2)} \approx 6.02. \tag{9.21b}$$

The $p \to 0$ behavior is $\lim_{p \to 0} \Delta_l(p) = e^2/2$, coincidentally the same limiting value $\Delta_v(0)$. The maximum value of the trailing edge speed $|s_+|$ is therefore

$$\max_{1 < \Delta < \Delta_s} |s_+| = u_1 + c_1 \left| \frac{4-p^2}{2p} \Delta_l(p)^{p/2} - \frac{2}{p} \right|, \qquad 0 < p < 1.$$

For $\Delta > \Delta_l(p)$, the simple wave construction is no longer valid.

For $0 < p < 1$, $\tilde{\alpha}(\Delta)$ exhibits singularity formation in its derivative when $\tilde{\alpha}(\Delta) \to -1/2$ for $\Delta \to \Delta_s(p)$, where

$$\Delta_s(p) = 2^{4/[p(3p-2)]} \left( \frac{1-p}{2+p} \right)^{4(1-p)/[p(3p-2)]}, \qquad 0 < p < 1, \qquad p \neq 2/3,$$
(9.22a)

$$\Delta_s(2/3) = 64 \exp(-9/4) \approx 6.75,$$
(9.22b)

so that DSWs with $\Delta > \Delta_s(p)$ are not admissible.

Based on the foregoing analysis and upon verification of the DSW edge ordering (6.1c), the modulation theory presented here does not violate any of the admissibility criteria for all $1 < \Delta$ when $p \geq 1$ and for $1 < \Delta < \Delta_1(p)$ when $0 < p < 1$.

### 9.2.1 Numerical Results

The simple wave DSW construction makes several predictions that can be tested through long-time numerical simulations of the shock tube problem of Sect. 5.3. For the details of the numerical method, see the appendix. Recall that the shock tube problem results in the generation of two waves, a DSW followed by a rarefaction wave. Figure 5a depicts the numerically computed density at $t = 350$ resulting from the initial jump $(\rho_1, \rho_2) = (1, 14)$ at $x = 2000$ for power-law gNLS with $p = 2/3$. The structure of a $1^+$-DSW connected to a 2-rarefaction via an intermediate, constant state is clear. Almost imperceptible modulations of the zoomed-in solution in the inset demonstrate the two-scale nature of dispersive hydrodynamics. Figure 5b provides a comparison of the intermediate density $\rho_m$ predicted by (5.14) (——), numerical computation (■, ▲, ●), and the intermediate density predicted for a classical, polytropic gas, equations (4.17) (----). The integrable NLS case $p = 1$ agrees precisely with the numerical computations, but for the nonintegrable cases, eventual deviation is observed for large initial jumps. Interestingly, the classical shock prediction begins to agree with the $p = 2$ numerics for sufficiently large jumps. Similar behavior was noted for gNLS with photorefractive nonlinearity (El et al. 2007) and for the Serre equations (El et al. 2006).

A comparison of the numerically extracted $1^+$-DSW speeds and simple DSW theory is shown in Fig. 6a, b. The speeds, resulting from simulations with different $p$ values, are normalized by the sound speed $c_1$. The value of the DSW jump $\Delta$ corresponding to the numerical simulation results (■, ▲, ●) is the one extracted from the computation; i.e., $\Delta$ is the numerical value of the density between the DSW and the rarefaction. The $\Delta$ value used for the theoretical predictions (——, ----) is $\rho_m$ from the shock tube problem (5.14). The computations for the integrable case $p = 1$ agree excellently, even for large jumps. The solid curves (——) show rapid deviation from the weak DSW straight line (----) predictions, signaling the importance of nonlinearity. In the weak to moderate jump regime $\Delta \lesssim 3$, the nonintegrable cases exhibit good agreement with the predicted soliton edge speed, but deviation occurs for large jumps. Interestingly, the nonintegrable cases admit excellent agreement with the predicted linear wave edge speed across their entire regions of validity.
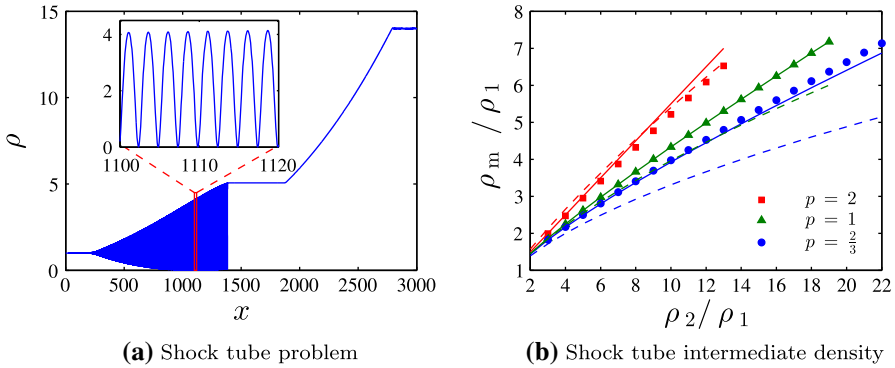
**(a)** Shock tube problem

**(b)** Shock tube intermediate density

**Fig. 5** **a** Density resulting from the numerical solution of the shock tube problem for power-law gNLS, $p = 2/3$. The inset depicts the slowly varying nature of the DSW. **b** Predicted (*solid lines*) and computed (*filled squares*, *filled triangles*, *filled circles*) intermediate states $\rho_m$ resulting from the shock tube problem. The prediction for a classical shock tube is also given (*dashed lines*)
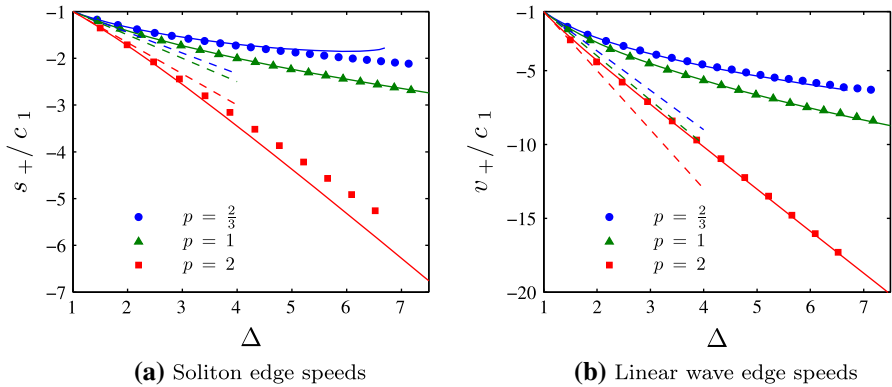


**(a)** Soliton edge speeds

**(b)** Linear wave edge speeds

**Fig. 6** Power-law gNLS 1-DSW speeds for varying density jump $\Delta$ and nonlinearity exponent $p$. *Solid lines* are from (9.16b), (9.16a), *filled squares*, *filled triangles*, and *filled circles* result from numerical simulation, and *dashed lines* show the weak DSW results (9.8a), (9.8b)

Recall that, for $p = 2/3$, linear degeneracy sets in for jump heights above that which corresponds to the minimum of the soliton edge speed curve (9.21b), $\Delta_l \approx 6$. However, the computed $1^+$-DSW shows no distinct change in structure for jumps below and above this threshold. This feature is depicted in Fig. 7. On the right, in regions in $(p, \Delta)$ space where a vacuum point is predicted to develop, the DSW modulation theory breaks down due to linear degeneracy, and singular behavior is shown. It is clear from this figure that $\Delta_v < \Delta_l < \Delta_s$ so that the simple wave condition has been broken due to linear degeneracy before singularity formation when $\Delta = \Delta_s$. Figure 7 (left) shows $1^+$-DSWs from numerical simulations for $p = 2/3$ and varying $\Delta$. A transition to cavitation is observed for sufficiently large jumps as predicted. However, in the linearly degenerate regime $\Delta > \Delta_l$, the simulation shows no noticeable change in the computed DSW structure.
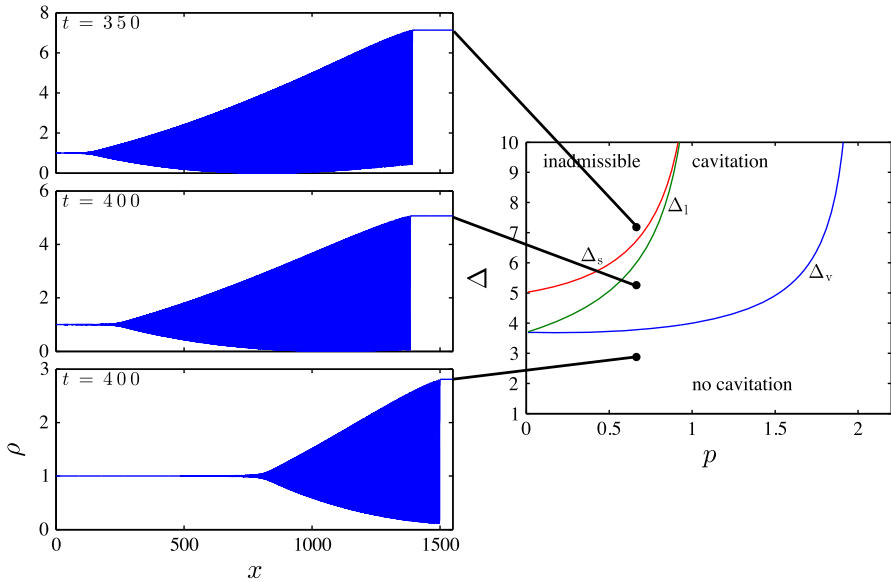
**Fig. 7** *Right* singular $\Delta > \Delta_s(p)$, linearly degenerate $\Delta_s(p) > \Delta > \Delta_1(p)$, and cavitation $\Delta_1(p) > \Delta > \Delta_v(p)$ regions in $(\Delta, p)$ phase space for a gNLS simple $1^+$-DSW with power-law $p$ nonlinearity. *Left* numerically computed $1^+$-DSWs for $p = 2/3$

The soliton minimum $\rho_{\min}$, determined by solving (9.9) with a numerical root finder, is shown in Fig. 8 for different choices of the nonlinearity $p$ and jump heights (curves). The simple DSW construction predicts no cavitation for $p > 2$ and a sharply increasing soliton minimum as the jump height is increased beyond $\Delta_v(2/3)$. Neither of these behaviors are observed numerically. Sufficiently large jumps in the $p = 2$ case lead to cavitation. The numerically computed density minima of the trailing edge soliton (■, ▲, ●), curiously, lie on the integrable NLS curve. It is not clear as to why this is the case.

### 9.3 Nonpolynomial Nonlinearity

Another particular form of nonlinearity is now considered, that of nonpolynomial non-linearity (3.3). When inserted into (9.3), this nonlinearity results in the nonseparable ODE parametrized by $\gamma$

$$\frac{d\alpha}{d\overline{\rho}} = -\frac{(1 + \alpha)[2 + 3\gamma\overline{\rho} + 2\alpha(2 + \gamma\overline{\rho})]}{4\overline{\rho}(1 + \gamma\overline{\rho})(1 + 2\alpha)}. \tag{9.23}$$

It is necessary to numerically solve (9.23) with the initial conditions (9.4), or (9.6) with $\alpha \to \tilde{\alpha}$, in order to recover DSW properties. Since

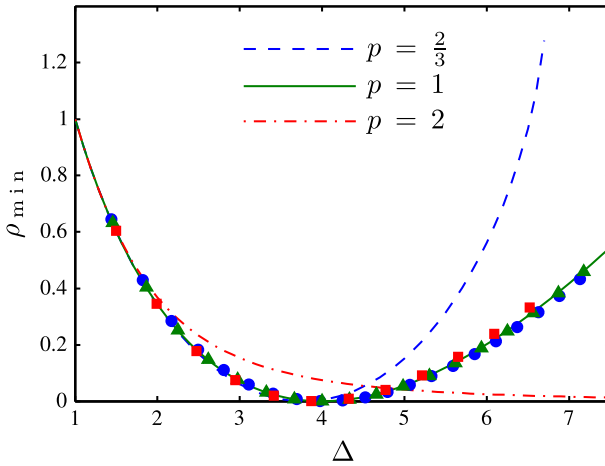**Fig. 8** Power-law gNLS DSW trailing soliton minimum $\rho_{\min}$ as a function of the DSW jump $\Delta$ and nonlinearity exponent $p$. Theory (*curves*) and numerics (*filled squares, filled triangles, filled circles*) significantly differ for $\Delta > \Delta_v$ and $p \neq 1$

$$\tilde{\alpha}_{\min}(\Delta) = -\frac{3}{2} + \frac{2}{2 + \gamma\Delta} < -\frac{1}{2}, \qquad \gamma\Delta > 0,$$

and $\tilde{\alpha}(\Delta)$ is a decreasing function for $\tilde{\alpha} > \tilde{\alpha}_{\min}$, singularity formation ($\tilde{\alpha} \to -1/2$) is guaranteed for $\gamma > 0$ and $\Delta$ sufficiently large. Linear degeneracy, however, occurs before this when

$$\tilde{\alpha}(\Delta_l) = -\frac{2 + \gamma\Delta_l}{4 + 4\gamma\Delta_l} > -\frac{1}{2}.$$

Note that, for $\gamma \gg 1$, the characteristic equation (9.23) asymptotes to the power-law nonlinearity equation (9.13) with $p = 1/2$ so that the behavior in the large-$\gamma$ limit can be recovered directly from (9.17a) and (9.18a).

Similar to the power-law nonlinearity, the three distinguished values for the shock jump $\Delta_v < \Delta_l < \Delta_s$ divide $(\gamma, \Delta)$ parameter space into various regions, as shown in Fig. 9. The large-$\gamma$ behavior of the distinguished values are, from (9.20a), (9.21a), and (9.22a) with $p = 1/2$,

$$\Delta_v(\gamma) \sim 3.7, \qquad \Delta_l(\gamma) \sim 5.1, \qquad \Delta_s(\gamma) \sim 6.0, \qquad \gamma \gg 1.$$

Cavitation and linear degeneracy are predicted to occur for $\gamma > 0$ with sufficiently large $\Delta$. Additionally, the small-$\gamma$ asymptotics can be determined as a regular perturbation to the NLS solution (9.17b). The result is complex so it is not reported here, deferring rather to the numerical solution of the ODE (9.23).
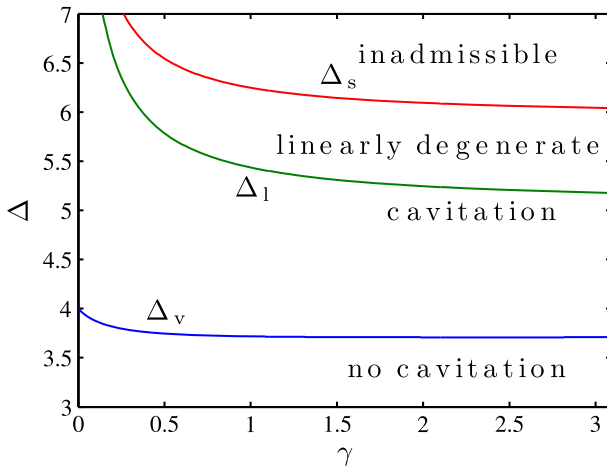
**Fig. 9** Singular $\Delta > \Delta_s(\gamma)$, linearly degenerate $\Delta_s(\gamma) > \Delta > \Delta_l(\gamma)$, and cavitation $\Delta_l(\gamma) > \Delta > \Delta_v(\gamma)$ regions for a simple wave led $1^+$-DSW with nonpolynomial nonlinearity
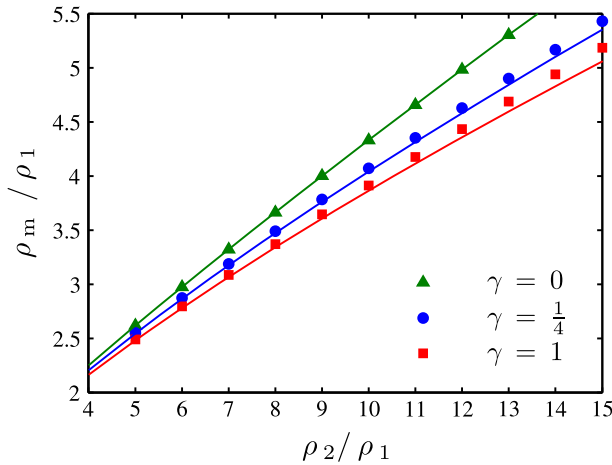


**Fig. 10** Predicted (*solid lines*) and computed (*filled squares*, *filled triangles*, *filled circles*) intermediate states $\rho_m$ resulting from the nonpolynomial gNLS shock tube problem

### 9.3.1 Numerical Results

The shock tube problem for $\gamma \in \{0, 1/4, 1\}$ was solved numerically. The resulting DSW shock structure exhibits a qualitatively similar pattern to the one shown in Fig. 5a. The computed intermediate density $\rho_m$, as compared with that resulting from the 1-DSW locus (5.14), is shown in Fig. 10. As before, when deviating from the integrable case with $\gamma > 0$, the 1-DSW locus provides a good prediction to the intermediate density for weak to moderate jumps but deviates in the large jump regime.

The computed DSW speeds are pictured in Fig. 11 for varying $\gamma$ and $\Delta$. The weak DSW results (- - - -) rapidly deviate from the predicted (——) and computed (■, ▲, ●)
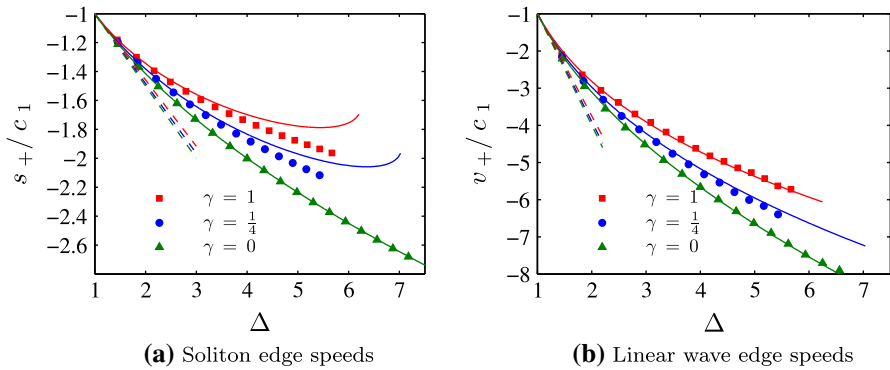
**Fig. 11** Nonpolynomial gNLS 1-DSW speeds for varying density jump $\Delta$ and parameter $\gamma$. *Solid curves* are from (9.16b), (9.16a), *filled squares*, *filled triangles*, and *filled circles* result from numerical simulation, and *dashed lines* show the weak DSW results (9.8a), (9.8b)
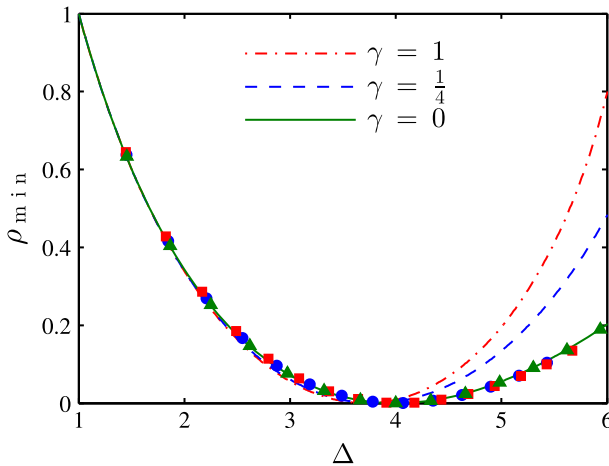


**Fig. 12** Soliton minimum $\rho_{\min}$ as a function of the DSW jump and nonpolynomial nonlinearity coefficient $\gamma$

results for $\Delta \gtrsim 1.5$. The nonintegrable DSW speeds with finite $\gamma$ deviate from the DSW regularization in the large jump regime $\Delta \gtrsim 3$, more so for the soliton edge speeds. The onset of linear degeneracy and singular behavior is clear from the solid soliton speed curves, exhibiting minima at $\Delta = \Delta_1(\gamma)$ and an infinite derivative at $\Delta = \Delta_s(\gamma)$.

The soliton minimum $\rho_{\min}$ is shown in Fig. 12. As with the power-law nonlinearity, the computed soliton trailing edge minima lie approximately on the integrable NLS curve, suggesting that this behavior is not coincidental to a particular type of nonlinearity chosen.
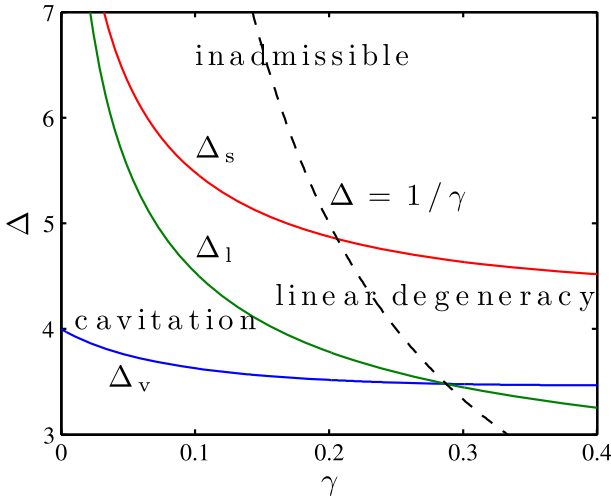
**Fig. 13** Validity of DSW modulation theory for photorefractive nonlinearity. The *dashed curve* corresponds to $c'(\Delta) = 0$

### 9.4 Photorefractive Media

The case of DSWs in photorefractive media (3.4) was studied in detail in El et al. (2007). There, the modulation theory was found to diverge for sufficiently large amplitude jumps and an explanation in terms of the existence of cavitation was given. Based on the theory developed in Sect. 6.2, this breakdown can be identified with linear degeneracy at the soliton edge, hence the simple wave condition no longer holds. A telltale sign of breakdown is realized by the extremum of the shock speed with respect to jump height in Fig. 7 of El et al. (2007). Figure 13 depicts the phase space $(\gamma, \Delta)$ divided into regions by the curves $\Delta_l(\gamma)$, $\Delta_v(\gamma)$, and $\Delta_s(\gamma)$. In contrast to the previous discussions, photorefractive nonlinearity only preserves the ordering $\Delta_v < \Delta_l < \Delta_s$ for $\gamma \lesssim 0.287$. However, the generic nonlinearity assumptions (3.7) corresponding to a convex pressure law or, equivalently, an increasing sound speed are violated for jumps exceeding $\Delta > 1/\gamma$. The dashed curve $\Delta = 1/\gamma$ shown in Fig. 13 demonstrates that the change in ordering of $\Delta_l$ and $\Delta_v$ occurs when $c'(\Delta) = 0$.

### 10 Large Amplitude DSWs with Negative Dispersion

Dispersive shock waves for fully nonlinear shallow water waves and ion-acoustic plasma have been studied elsewhere El (2005); El et al. (2006). It is worth commenting on these results in light of the theory presented here. Both systems exhibit alternative negative dispersion regularizations of the Euler equations in contrast to the positive dispersion of gNLS.

In shallow water with zero surface tension $\sigma = 0$ (El et al. 2006), the linear degeneracy condition (6.14) occurs at the trailing edge for relatively small jumps $\Delta = \Delta_l \approx 1.43$. For $\Delta > \Delta_l$, the simple wave theory breaks down and, indeed,

the numerically computed soliton edge speed begins to deviate noticeably from its theoretical value (see Figs. 3 and 4 in El et al. (2006)). It is curious that the numerically computed linear edge speed remains fairly accurate. For $\sigma = 0$, zero dispersion does not occur at either edge, nor does linear degeneracy at the soliton edge. For $\sigma > 0$, both $\omega_{kk} = 0$ and $(\tilde{\omega}/\tilde{k})_{\tilde{k}} = 0$ when $\rho = \sqrt{3\sigma}$, offering a potential route to gradient catastrophe in the Whitham modulation equations for appropriate DSW jumps.

Ion-acoustic plasma DSWs also exhibit linear degeneracy at the linear wave edge for appropriate jump heights. The linear edge speed plotted in Fig. 5 of El (2005) for a $2^-$-DSW from $\rho_1 = \Delta$ to $\rho_2 = 1$ exhibits the requisite minimum as $\Delta$ is varied [recall (6.19b)]. A numerical computation shows that the minimum occurs when $\Delta = \Delta_1 \approx 1.41$. Zero dispersion at either edge and linear degeneracy at the soliton edge do not occur by calculation of the criteria from Sect. 6.2.

The particular dispersive Eulerian fluids discussed here demonstrate the importance of the breakdown criteria (6.19a), (6.19b) in both negative and positive dispersion cases.

# 11 Conclusions

Shock waves in the dispersively regularized isentropic Euler $P$-system under modest assumptions were constructed using the Whitham–El simple wave closure technique. A complete, explicit characterization of admissible, weak DSWs was shown to depend only on the pressure law and convexity or concavity of the dispersion relation. Linear degeneracy of the modulation equations and zero dispersion leading to gradient catastrophe in the modulation equations were identified as causes of the breakdown of the simple wave assumption. Simple tests in terms of extrema of the DSW leading or trailing edge speeds for these behaviors were elucidated. Large amplitude DSWs were constructed for the case of the gNLS equation modeling super and optical fluids. Comparisons with careful numerical simulations of the shock tube problem reveal excellent agreement with theory in the weak to moderate jump regime. Deviation occurred in the large jump regime with linear degeneracy in the modulation equations at the DSW soliton edge a proximate cause for certain pressure laws.

While there are a number of parallels between classical, viscous Eulerian fluids and dispersive Eulerian fluids, this work has demonstrated that DSWs exhibit distinct physical and mathematical behavior. Physically, the generation of oscillations leads to an expanding oscillatory region with two speeds in contrast to localized, classical shock fronts propagating as traveling waves. Positive dispersion fluids can exhibit DSWs with cavitation, while negative dispersion fluids admit DSWs with backflow. Mathematically, weak Eulerian DSWs and shocks exhibit universal behavior, depending only upon the sign of dispersion and the pressure law. In the large amplitude regime, universality is maintained for classical viscous shock jump conditions, which are the same for a large class of dissipative regularizations. However, due to their nonlocal nature and the weak limit involved, large amplitude DSWs crucially depend upon the particular form of the dispersion. Furthermore, admissibility of simple wave led DSWs is much more subtle than the elegantly stated Lax entropy conditions for classical shocks.

## Appendix: Numerical Methods

The numerical solution of the gNLS equation (3.1) for the shock tube problem, the initial step in density

$$\psi(x, 0) = \begin{cases} 1 & x < x_0 \\ \sqrt{\rho_2} & x > x_0 \end{cases}, \qquad \rho_2 > 1, \tag{11.1}$$

is briefly described here. A pseudospectral, time-splitting method is implemented for the accurate solution of long-time evolution for $x \in (0, L)$. The initial data (11.1) are smoothed by use of the hyperbolic tangent initial condition

$$\psi(x, 0) = \left\{ \frac{1}{2}[1 + \tanh(x_0 - x)](1 - \rho_2) + \rho_2 \right\}^{1/2},$$

where $x_0 = L/2$. Time stepping proceeds by use of second-order Strang splitting Strang (1968) where the linear PDE

$$i\frac{\partial \psi_L}{\partial t} = -\frac{1}{2}\frac{\partial^2 \psi_L}{\partial x^2}, \qquad \psi_L(x, t) = \psi(x, t), \tag{11.2}$$

is advanced half a time step $\Delta t/2$ exactly followed by a full time step of the nonlinear ODE

$$i\frac{\partial \psi_{NL}}{\partial t} = f(|\psi_{NL}|^2)\psi_{NL}, \qquad \psi_{NL}(x, t) = \psi_L(x, t + \Delta t/2). \tag{11.3}$$

The linear PDE is then advanced half a time step with the initial data $\psi_L(x, t + \Delta t/2) = \psi_{NL}(x, t + \Delta t)$, giving the second-order accurate approximation of $\psi(x, t + \Delta t) \approx \psi_L(x, \Delta t)$. Equation (11.2) is projected onto a truncated cosine basis of $N$ terms that maintains Neumann ($\psi_x = 0$) boundary conditions, computed efficiently via the fast Fourier transform (FFT), and integrated explicitly in time. The nonlinear ODE (11.3) conserves $|\psi_{NL}|^2$ so is also integrated explicitly in time. The parameter $\Delta x = L/N$ is the spatial grid spacing of the grid points $x_j = \Delta x(j - 1/2)$, $j = 1, 2, \ldots, N$. The accuracy of the solution is monitored by computing the relative deviation in the conserved $L^2$ norm $E(t) = \int_{\mathbb{R}} |\psi(x, t)|^2 \mathrm{d}x$, $E_{rel} = |E(t_f) - E(0)|/E(0)$ where $t_f$ is the final time. All computations presented here exhibit $E_{rel} < 10^{-8}$. Also, the accurate spatial resolution of the oscillatory structures is supported by the fact that the coefficient of the largest wavenumber in the cosine series is less than $5 \cdot 10^{-10}$ (oftentimes much less). The numerical parameters $L$, $N$, $\Delta t$, and $t_f$ vary depending upon the nonlinearity strength and jump height; For example, for power-law gNLS with $p = 2$ and $\rho_2 \geq 11$, $N = 2^{16}$, $L = 1,200$, $\Delta t = 0.0002$, and $t_f = 30$, whereas for $p = 2/3$ with $\rho_2 = 2$, $N = 3 \cdot 2^{14}$, $L = 3,000$, $\Delta t = 0.002$, and $t_f = 500$.

The extraction of the DSW speeds $v_+$, $s_+$, and minimum density $\rho_{\min}$ is performed as follows: The precise location of the DSW soliton trailing edge is computed by creating a local cubic spline interpolant through the computed grid points in the neighborhood of the dark soliton minimum. A root finder is applied to the derivative of this interpolant in order to extract the off-grid location of the soliton edge $x_s(t)$ and $\rho_{\min} \equiv |\psi(x_s(t_f), t_f)|^2$. The slope of a linear least-squares fit through $x_s(t_j)$ for $j = 1, \ldots, 100$ equispaced $t_j \in [t_f - 1, t_f]$ determines $s_+$. For the leading, linear wave edge, an envelope function is determined by least-squares fitting two lines, each through about 30 local maxima and minima, respectively, of the DSW density in the vicinity of the trailing edge. The extrema are computed the same as for the soliton minimum. The point of intersection of these two lines is the location of the linear wave edge $x_v(t)$. The same fitting procedure as was used to determine $s_+$ from $x_s(t)$ is used to extract $v_+$ from $x_v(t)$.

# References

Ablowitz, M.J., Baldwin, D.E., Hoefer, M.A.: Soliton generation and multiple phases in dispersive shock and rarefaction wave interaction. Phys. Rev. E **80**(1), 016603 (2009)

Barsi, C., Wan, W., Sun, C., Fleischer, J.W.: Dispersive shock waves with nonlocal nonlinearity. Opt. Lett. **32**(20), 2930–2932 (2007)

Barsi, C., Wan, W., Jia, S., Fleischer, J.: Spatially dispersive shock waves in nonlinear optics. In: Chen, Z., Morandotti, R. (eds.) Nonlinear Photonics and Novel Optical Phenomena. Springer Series in Optical Sciences, vol. 170, pp. 231–257. Springer, Berlin/Heidelberg (2012)

Biondini, G., Kodama, Y.: On the Whitham equations for the defocusing nonlinear Schroödinger equation with step initial data. J. Nonlinear Sci. **16**, 435–481 (2006)

Chang, J.J., Engels, P., Hoefer, M.A.: Formation of dispersive shock waves by merging and splitting Bose-Einstein condensates. Phys. Rev. Lett. **101**, 170404 (2008)

Chanson, H.: Current knowledge in hydraulic jumps and related phenomena: a survey of experimental results. Eur. J. Mech. B **28**(2), 191–210 (2009)

Chen, T., Pavlovic, N.: The quintic NLS as the mean field limit of a boson gas with three-body interactions. J. Funct. Anal. **260**(4), 959–997 (2011)

Christie, D.R.: The morning glory of the Gulf of Carpentaria: a paradigm for non-linear waves in the lower atmosphere. Austral. Met. Mag. **41**, 21–60 (1992)

Christodoulides, D.N., Carvalho, M.I.: Bright, dark, and gray spatial soliton states in photorefractive media. J. Opt. Soc. Am. B **12**(9), 1628–1633 (1995)

Conforti, M., Baronio, F., Trillo, S.: Dispersive shock waves in phase-mismatched second-harmonic generation. Opt. Lett. **37**(6), 1082–1084 (2012)

Conti, C., Fratalocchi, A., Peccianti, M., Ruocco, G., Trillo, S.: Observation of a gradient catastrophe generating solitons. Phys. Rev. Lett. **102**(8), 083902 (2009)

Courant, R., Friedrichs, K.O.: Supersonic Flow and Shock Waves. Springer, New York (1948)

Crosta, M., Fratalocchi, A., Trillo, S.: Bistability and instability of dark-antidark solitons in the cubic-quintic nonlinear Schroödinger equation. Phys. Rev. A **84**(6), 011604 (2011)

Crosta, M., Trillo, S., Fratalocchi, A.: Crossover dynamics of dispersive shocks in Bose-Einstein condensates characterized by two- and three-body interactions. Phys. Rev. A **85**(4), 011604 (2012)

Crosta, M., Trillo, S., Fratalocchi, A.: The Whitham approach to dispersive shocks in systems with cubic-quintic nonlinearities. New J. Phys. **14**(9), 093019 (2012)

Csordás, A., Almásy, O., Szépfalusy, P.: Gradient corrections to the local-density approximation for trapped superfluid Fermi gases. Phys. Rev. A **82**(6), 063609 (2010)

Dafermos, C.M.: Hyperbolic Conservation Laws in Continuum Physics, 3rd edn. Springer, New York (2009)

Dias, F., Milewski, P.: On the fully-nonlinear shallow-water generalized Serre equations. Phys. Lett. A **374**(8), 1049–1053 (2010)

Dutton, Z., Budde, M., Slowe, C., Hau, L.V.: Observation of quantum shock waves created with ultra-compressed slow light pulses in a Bose-Einstein condensate. Science **293**, 663 (2001)

El, G.A., Krylov, A.L.: General solution of the Cauchy problem for the defocusing NLS equation in the Whitham limit. Phys. Lett. A **203**, 77–82 (1995)

El, G.A., Geogjaev, V.V., Gurevich, A.V., Krylov, A.L.: Decay of an initial discontinuity in the defocusing NLS hydrodynamics. Phys. D **87**, 186–192 (1995)

El, G.A.: Generating function of the Whitham-KdV hierarchy and effective solution of the Cauchy problem. Phys. Lett. A **222**, 393–399 (1996)

El, G.A.: Resolution of a shock in hyperbolic systems modified by weak dispersion. Chaos **15**, 037103 (2005)

El, G.A., Grimshaw, R.H.J., Smyth, N.F.: Unsteady undular bores in fully nonlinear shallow-water theory. Phys. Fluids **18**(2), 027104–027117 (2006)

El, G.A., Gammal, A., Khamis, E.G., Kraenkel, R.A., Kamchatnov, A.M.: Theory of optical dispersive shock waves in photorefractive media. Phys. Rev. A **76**(5), 053813 (2007)

Esler, J.G., Pearce, J.D.: Dispersive dam-break and lock-exchange flows in a two-layer fluid. J. Fluid Mech. **667**, 555–585 (2011)

Forest, M.G., McLaughlin, K.T.-R.: Onset of oscillations in nonsoliton pulses in nonlinear dispersive fibers. J. Nonlinear Sci. **8**(1), 43–62 (1998)

Gavrilyuk, S.L.: Large amplitude oscillations and their 'thermodynamics' for continua with 'memory'. Eur. J. Mech. B **13**, 753–764 (1994)

Gavrilyuk, S.L., Teshukov, V.M.: Generalized vorticity for bubbly liquid and dispersive shallow water equations. Contin. Mech. Therm. **13**, 365–382 (2001)

Ghofraniha, N., Conti, C., Ruocco, G., Trillo, S.: Shocks in nonlocal media. Phys. Rev. Lett. **99**, 043903 (2007)

Ghofraniha, N.: Amato Santamaria, L., Folli, V., Trillo, S., DelRe, E., Conti, C.: Measurement of scaling laws for shock waves in thermal nonlocal media. Opt. Lett. **37**(12), 2325–2327 (2012)

Giorgini, S., Pitaevskii, L.P., Stringari, S.: Theory of ultracold atomic Fermi gases. Rev. Mod. Phys. **80**(4), 1215 (2008)

Grava, T., Tian, F.-R.: The generation, propagation, and extinction of multiphases in the KdV zero-dispersion limit. Commun. Pure Appl. Math. **55**(12), 1569–1639 (2002)

Grava, T., Pierce, V.U., Tian, F.-R.: Initial value problem of the Whitham equations for the Camassa-Holm equation. Phys. D **238**(1), 55–66 (2009)

Green, A.E., Naghdi, P.M.: A derivation of equations for wave propagation in water of variable depth. J. Fluid Mech. **78**(02), 237–246 (1976)

Gurevich, A.V., Pitaevskii, L.P.: Nonstationary structure of a collisionless shock wave. Sov. Phys. JETP 38(2), 291–297 (1974). (Translation from Russian of A. V. Gurevich and L. P. Pitaevskii. Zh. Eksp. Teor. Fiz. **65**, 590–604 (1973)

Gurevich, A.V., Meshcherkin, A.P.: Expanding self-similar discontinuities and shock waves in dispersive hydrodynamics. Sov. Phys. JETP **60**(4), 732–740 (1984)

Gurevich, A.V., Krylov, A.L.: Dissipationless shock waves in media with positive dispersion. Sov. Phys. JETP **65**(5), 944–953 (1987)

Gurevich, A.V., Krylov, A.L., El, G.A.: Nonlinear modulated waves in dispersive hydrodynamics. Sov. Phys. JETP **71**, 899–910 (1990)

Hoefer, M.A., Ablowitz, M.J., Coddington, I., Cornell, E.A., Engels, P., Schweikhard, V.: Dispersive and classical shock waves in Bose-Einstein condensates and gas dynamics. Phys. Rev. A **74**, 023623 (2006)

Hoefer, M.A., Ablowitz, M.J.: Interactions of dispersive shock waves. Phys. D **236**, 44–64 (2007)

Hoefer, M.A., Ablowitz, M.J.: Dispersive shock waves. Scholarpedia **4**(11), 5562 (2009)

Holloway, P., Pelinovsky, E., Talipova, T.: Internal tide transformation and oceanic internal solitary waves. In: Grimshaw, R.H.J. (ed.) Environmental Stratified Flows, pp. 29–60. Kluwer, Boston (2001)

Jia, S., Wan, W., Fleischer, J.W.: Dispersive shock waves in nonlinear arrays. Phys. Rev. Lett. **99**(22), 223901–223904 (2007)

Jia, S., Haataja, M., Fleischer, J.W.: Rayleigh-Taylor instability in nonlinear Schroödinger flow. New J. Phys. **14**(7), 075009 (2012)

Jin, S., Levermore, C.D., McLaughlin, D.W.: The semiclassical limit of the defocusing NLS hierarchy. Commun. Pure Appl. Math. **52**(5), 613–654 (1999)

Joseph, J.A., Thomas, J.E., Kulkarni, M., Abanov, A.G.: Observation of shock waves in a strongly interacting Fermi gas. Phys. Rev. Lett. **106**(15), 150401 (2011)

Kamchatnov, A.M., Kuo, Y.-H., Lin, T.-C., Horng, T.-L., Gou, S.-C., Clift, R., El, G.A., Grimshaw, R.H.J.: Undular bore theory for the Gardner equation. Phys. Rev. E **86**, 036605 (2012)

Karpman, V.I.: Non-linear Waves in Dispersive Media. Pergamon, Oxford (1974)

Ketterle, W., Zwierlein, M.W.: Making, probing and understanding ultracold Fermi gases. Riv. Nuovo Cimento **31**(5), 247–422 (2008)

Kevrekidis, P.G., Frantzeskakis, D.J., Carretero-Gonzlez, R.: Emergent Nonlinear Phenomena in Bose-Einstein Condensates: Theory and Experiment. Springer Series on Atomic, Optical, and Plasma Physics, vol. 45, pp. 1615–5653. Springer, Berlin (2008).

Khamis, E.G., Gammal, A., El, G.A., Yu, G.G., Kamchatnov, A.M.: Nonlinear diffraction of light beams propagating in photorefractive media with embedded reflecting wire. Phys. Rev. A **78**(1), 013829 (2008)

Kodama, Y., Pierce, V.U., Tian, F.-R.: On the Whitham equations for the defocusing complex modified KdV equation. SIAM J. Math. Anal. **41**(1), 26–58 (2008)

Lax, P.D.: Development of singularities of solutions of nonlinear hyperbolic partial differential equations. J. Math. Phys. **5**(5), 611–613 (1964)

Lax, P.D.: Hyperbolic Systems of Conservation Laws and the Mathematical Theory of Shock Waves. SIAM, Philadelphia (1973)

Lax, P.D., Levermore, C.D.: The small dispersion limit of the Korteweg-de Vries equation: 1. Commun. Pure Appl. Math. **36**(3), 253–290 (1983)

Lax, P.D., Levermore, C.D.: The small dispersion limit of the Korteweg-de Vries equation: 2. Commun. Pure Appl. Math. **36**(5), 571–593 (1983)

Lax, P.D., Levermore, C.D.: The small dispersion limit of the Korteweg-de Vries equation: 3. Commun. Pure Appl. Math. **36**(6), 809–830 (1983)

Leach, J.A., Needham, D.J.: The large-time development of the solution to an initial-value problem for the Korteweg-de Vries equation: I. initial data has a discontinuous expansive step. Nonlinearity **21**(10), 2391–2408 (2008)

Liepmann, H.W., Roshko, A.: Elements of Gas Dynamics. Wiley, New York (1957)

Lowman, N.K., Hoefer, M.A.: Dispersive shock waves in viscously deformable media. J. Fluid Mech. **718**, 524–557 (2013)

Madelung, E.: Quantentheorie in hydrodynamischer form. Zeitschrift fur Physik **40**(3–4), 322–326 (1927)

Marchant, T., Smyth, N.: Undular bore solution of the Camassa-Holm equation. Phys. Rev. E **73**(5), 057602 (2006)

Mateo, Muaz: A.: Effective mean-field equations for cigar-shaped and disk-shaped Bose-Einstein condensates. Phys. Rev. A 77(1), 013617 (2008).

Meppelink, R., Koller, S.B., Vogels, J.M., van der Straten, P., van Ooijen, E.D., Heckenberg, N.R., Rubinsztein-Dunlop, H., Haine, S.A., Davis, M.J.: Observation of shock waves in a large Bose-Einstein condensate. Phys. Rev. A **80**(4), 043606–043607 (2009)

Novikov, S., Manakov, S.V., Pitaevskii, L.P., Zakharov, V.E.: Theory of Solitons. Consultants Bureau, New York (1984)

Pierce, V.U., Tian, F.-R.: Self-similar solutions of the non-strictly hyperbolic Whitham equations. Commun. Math. Sci. **4**, 799–822 (2006)

Pierce, V.U., Tian, F.-R.: Large time behavior of the zero dispersion limit of the fifth order KdV equation. Dyn. PDE **4**(1), 87–109 (2007)

Pierce, V.U., Tian, F.-R.: Self-similar solutions of the non-strictly hyperbolic Whitham equations for the KdV hierarchy. Dyn. PDE **4**(3), 263–282 (2007)

Rottman, J.W., Grimshaw, R.H.J.: Atmospheric internal solitary waves. In: Grimshaw, R.H.J. (ed.) Environmental Stratified Flows, pp. 61–88. Kluwer, Boston (2001)

Salasnich, L., Parola, A., Reatto, L.: Effective wave equations for the dynamics of cigar-shaped and disk-shaped Bose condensates. Phys. Rev. A **65**(4), 043614 (2002)

Salasnich, L.: Dynamical properties of the unitary Fermi gas: collective modes and shock waves. Few-Body Syst. (2012). doi:10.1007/s00601-012-0442-y

Segev, M., Crosignani, B., Yariv, A., Fischer, B.: Spatial solitons in photorefractive media. Phys. Rev. Lett. **68**(7), 923 (1992)

Serre, F.: Contribution a l'etude des ecoulements permanents et variables dans les canaux. La Houille Blanche **3**, 374–388 (1953)

Simula, T.P., Engels, P., Coddington, I., Schweikhard, V., Cornell, E.A., Ballagh, R.J.: Observations on sound propagation in rapidly rotating Bose-Einstein condensates. Phys. Rev. Lett. **94**, 080404 (2005)

Smith, R.K.: Waves and bores in the lower atmosphere: the "morning glory" and related phenomena. Earth-Sci. Rev. **25**, 1501–1518 (1988)

Smoller, J.: Shock Waves and Reaction-Diffusion Equations. Springer, New York (1994)

Strang, G.: On the construction and comparison of difference schemes. SIAM J. Numer. Anal. **5**(3), 506–517 (1968)

Su, C.H., Gardner, C.S.: Korteweg-deVries equation and generalizations. III. Derivation of the Korteweg-deVries equation and Burgers equation. J. Math. Phys. **10**(3), 536–539 (1969)

Sulem, C., Sulem, P.-L.: The Nonlinear Schrödinger Equation. Springer, New York (1999)

Taylor, R.J., Baker, D.R., Ikezi, H.: Observation of collisionless electrostatic shocks. Phys. Rev. Lett. **24**, 206–209 (1970)

Temple, B.: Systems of conservation laws with coinciding shock and rarefaction curves. Contemp. Math **17**(143), 151 (1983)

Tsarev, S.P.: Poisson brackets and one-dimensional Hamiltonian systems of hydrodynamic type. Sov. Math. Dokl. **31**, 488–491 (1985)

Venakides, S.: The zero-dispersion limit of the Korteweg-de Vries equation with non-trivial reflection coefficient. Commun. Pure Appl. Math. **38**, 125–155 (1985)

Wagner, D.H.: Equivalence of the Euler and Lagrangian equations of gas dynamics for weak solutions. J. Diff. Equ. **68**(1), 118–136 (1987)

Wan, W., Jia, S., Fleischer, J.W.: Dispersive superfluid-like shock waves in nonlinear optics. Nat. Phys. **3**(1), 46–51 (2007)

Wan, W., Muenzel, S., Fleischer, J.W.: Wave tunneling and hysteresis in nonlinear junctions. Phys. Rev. Lett. **104**(7), 073903 (2010)

Whitham, G.B.: Non-linear dispersive waves. Proc. R. Soc. Ser. A **283**, 238–261 (1965)

Whitham, G.B.: Linear and Nonlinear Waves. Wiley, New York (1974)

Wijngaarden, L.V.: One-dimensional flow of liquids containing small gas bubbles. Annu. Rev. Fluid Mech. **4**, 369–396 (1972)